Distinct evolutionary trajectories of neuronal and hair cell nicotinic acetylcholine receptors

Irina Marcovich[1], Marcelo J. Moglie[1], Agustín E. Carpaneto Freixas[1], Anabella Trigila[1], Lucia F. Franchini[1], Paola V. Plazas[2], Marcela Lipovsek*[1,3] and Ana Belén Elgoyhen*[1,2]

[1] Instituto de Investigaciones en Ingeniería Genética y Biología Molecular "Dr. Héctor N. Torres" (INGEBI), Consejo Nacional de Investigaciones Científicas y Técnicas (CONICET), Buenos Aires, Argentina.

[2] Instituto de Farmacología, Facultad de Medicina, Universidad de Buenos Aires, Buenos Aires, Argentina.

[3] Centre for Developmental Neurobiology, King's College London, Institute of Psychiatry, Psychology and Neuroscience, Guy's Campus, London SE1 1UL.

*These authors contributed equally.

Correspondence should be addressed to Marcela Lipovsek (marcela.lipovsek@kcl.ac.uk)

ABSTRACT

The expansion and pruning of ion channel families has played a crucial role in the evolution of nervous systems. Remarkably, with a highly conserved vertebrate complement, nicotinic acetylcholine receptors (nAChRs) are unique among ligand-gated ion channels in that distinct members of the family have non-overlapping roles in synaptic transmission, either in the nervous system, the inner ear hair cells or the neuromuscular junction. Here, we performed a comprehensive analysis of vertebrate nAChRs sequences, single cell expression patterns and comparative functional properties of receptors from three representative tetrapod species. We show that hair cell nAChRs underwent a distinct evolutionary trajectory to that of neuronal receptors. These were most likely shaped by different co-expression patterns and co-assembly rules of component receptor subunits. Thus, neuronal nAChRs showed high degree of coding sequence conservation, coupled to greater co-expression variance and conservation of functional properties across tetrapod clades. In contrast, hair cell α9α10 nAChRs exhibited greater sequence divergence, narrow co-expression pattern and great variability of functional properties across species. These results point to differential substrates for random change within the family of gene paralogs that relate to the segregated roles of nAChRs in synaptic transmission.

INTRODUCTION

The superfamily of pentameric ligand-gated ion channels (LGIC) has an extended evolutionary history and is present in all three life domains (Dent, 2006; Jaiteh et al., 2016; Tasneem et al., 2005). Extant members of the superfamily include eukaryote Cys-loop receptors that respond to acetylcholine (ACh), γ-aminobutyric acid (GABA), glycine or serotonin, invertebrate LGICs that respond to GABA, glutamate, ACh, serotonin and histamine, as well as prokaryote pH and GABA sensitive receptors, among others (Bocquet et al., 2009; Cully et al., 1994; Dent, 2006; Hervé Thany, 2010; Hilf and Dutzler, 2009; Karlin, 2002; Pan et al., 2012; Spurny et al., 2012; Tasneem et al., 2005; Zheng et al., 2002). Nicotinic acetylcholine receptors (nAChRs) are a major branch of the Cys-loop LGIC superfamily (Corringer et al., 2012; Karlin, 2002). To date, 17 different nAChR subunits have been described in the main vertebrate clades: α1-α10, β1-β4, δ, ε and γ (Lester et al., 2004; Millar and Gotti, 2009). These paralogous genes are proposed to derive from 5 paralogons, with the entire complement of extant subunits present in the vertebrate ancestor (Pedersen et al., 2019). Vertebrate nAChRs are non-selective cation channels that participate in numerous processes, most prominently neuromuscular junction (Kalamida et al., 2007; Steinbach, 1989), inner ear efferent (Elgoyhen and Katz, 2012) and neuronal (Albuquerque et al., 2009; Dani and Bertrand, 2007; Zoli et al., 2015) synaptic transmission.

Functional nAChRs are homomeric, comprising five identical subunits, or heteromeric, formed by at least two different subunits (Karlin, 2002; Millar and Gotti, 2009; Zoli et al., 2015). The rules that govern the combinatorial assembly of functional nAChRs are complex and for the most part unknown. Some nAChR subunits can combine with other numerous, albeit specific, subunits. In contrast, some subunits can only form functional receptors with a limited subset (Karlin, 2002; Millar and Gotti, 2009). This segregation has given rise to the three traditional subgroups of vertebrate nAChRs, neuronal, muscle and hair cell, named for their initially described tissue of origin and main functional location. Thus, neuronal nAChRs are formed by multiple combinations of α2-α7 (and α8 in non-mammals) and β2-β4 subunits, comprising a wide combinatorial range with alternative stoichiometries (Millar and Gotti, 2009; Zoli et al., 2015; Zoli et al., 2018). Muscle receptors show tighter co-assembly rules. They have a typical $\alpha1_2\beta1\gamma\delta$ (or $\alpha1_2\beta1\varepsilon\delta$) stoichiometry and do not co-assemble with non-muscle subunits (Millar and Gotti, 2009; Mishina et al., 1986). Finally, the hair cell nAChR has a very strict co-assembly constraint, being formed exclusively by α9 and α10 subunits (Elgoyhen et al., 1994; Elgoyhen et al., 2001; Scheffer et al., 2007; Sgard et al., 2002). While α9 subunits can form functional homomeric receptors (Elgoyhen et al., 1994; Lipovsek et al., 2014), these are unlikely to play a major role in inner ear hair cells in vivo (Vetter et al., 2007). A consequence of the differences in co-assembly rules between the three subgroups of nAChRs is that,

while muscle cells can toggle between at least two receptor variants and neurons are capable of expressing a great diversity of nAChRs, hair cells express only one type.

The complement of nAChR subunits is highly conserved across vertebrates and even more so in tetrapods (Dent, 2006; Pedersen et al., 2019). This suggests a high gene family-wide negative selection pressure for the loss of paralogs and highlights the functional relevance of each individual subunit across the vertebrate clade. However, given the major differences in co-expression patterns and co-assembly rules that distinguish the subgroups of nAChRs, in particular the contrast between neuronal and hair cell receptors, distinct evolutionary trajectories most likely took place in different members of the family. On the one hand, if only one (functionally isolated) receptor is expressed by a given cell type, then selection pressure could have acted on stochastic changes of the coding sequence of component subunits that altered receptor function. Such changes would not have resulted in deleterious effects on other nAChRs given the restricted expression pattern of the subunits. The aforesaid process could have dominated the evolutionary history of the hair cell α9α10 receptor. On the other hand, widely expressed subunits that co-assemble into functional receptors with multiple others have been most probably subjected to strong negative selection pressure. Changes in the coding sequence that led to changes in functional properties may have had deleterious effects on alternative receptor combinations expressed in different cell types. In this case, functional diversification could have arisen from stochastic changes in the expression patterns of receptor subunits, resulting in a given cell changing the subtype of receptor it expresses, while preserving individual subunit functionality. Such processes could have dominated the evolutionary history of neuronal nAChRs. These contrasting theoretical scenarios bring forward three predictions for the evolutionary history of nAChRs across the vertebrate clade. First, isolated (hair cell) subunits may show coding sequence divergence while widespread (neuronal) subunits a high degree of coding sequence conservation. Second, isolated subunits may show low co-expression variation while widespread subunits a great variability in co-expression patterns. Finally, isolated receptors may present divergent functional properties across species resulting from changes in coding sequences, while widespread receptors may show highly conserved functional properties when formed by the same subunits.

To test these predictions, we studied the molecular phylogeny and the variability in expression pattern, coupled to co-assembly potential, of vertebrate nAChR subunits. Furthermore, we performed a comprehensive comparative analysis of the functional properties of the hair cell (α9α10) and the two main neuronal (α7 and α4β2) nAChRs from three representative species of tetrapods. In close agreement with the aforementioned predictions, neuronal subunits showed high degree of sequence conservation and great variability in co-expression patterns. Additionally, the

103 functional properties of both α7 and α4β2 receptors did not differ across tetrapods. In contrast, the
104 isolated hair cell α9α10 nAChRs showed the highest degree of sequence divergence and no co-
105 expression variability. Moreover, the functional properties of α9α10 receptors from representative
106 species of tetrapods showed unprecedented divergence, potentially echoing the evolutionary history
107 of vertebrate auditory systems. In summary, here we present strong evidence supporting the notion
108 that, within the family of paralog genes coding for nAChR subunits, receptors belonging to different
109 subgroups (hair cell or neuronal) underwent different evolutionary trajectories along the tetrapod
110 lineage that were potentially shaped by their different co-expression patterns and co-assembly rules.
111 Furthermore, we propose that it is the difference in the most probable substrate for random change
112 and subsequent selection pressure that separate the contrasting evolutionary histories of nAChRs
113 subgroups.

114

115 **RESULTS**

116 **Amino acid sequence divergence and co-expression patterns differentiate neuronal from hair cell**
117 **nAChR subunits**

118 The comparative analysis of gene paralogs provides the opportunity to test predictions about the
119 evolutionary history of a gene family. In order to study the degree of conservation of coding
120 sequences in subgroups of nAChRs, we performed an exhaustive evaluation of the sequence identity
121 of vertebrate nAChR subunits. The analysis included amino acid sequences from 11 species of birds,
122 reptiles and amphibians , all groups that were notably under-represented in previous work (Dent,
123 2006; Franchini and Elgoyhen, 2006; Le Novère et al., 2002; Lipovsek et al., 2012; Ortells and Lunt,
124 1995; Tsunoyama and Gojobori, 1998). The incorporation of these sequences is of particular
125 importance to help resolve differences between clades. Overall, we analysed 392 sequences from 17
126 nAChR subunits belonging to 29 vertebrate species (Supplementary Table 1). Amino acid sequences
127 were aligned with *Clustal*W (Supplementary File 1) and a minimum evolution tree was generated
128 (Figure 1 and Supplementary Figures 1-2). Based on sequence identity, the family of nAChR subunits
129 can be split into four groups: α, non-α, α7-like and α9-like (Figure 1). Neuronal subunits (α2-α8 and
130 β2-β4) have the highest degree of vertebrate-wide sequence conservation as observed by the
131 overall, within and between clade comparisons (Figure 1 – bar graphs and Table 1). Percentage
132 sequence identities (%seqIDs) between neuronal orthologues ranged between 72-84% (Figure 1 and
133 Table 1). Moreover, %seqIDs for neuronal subunits within and between mammals and sauropsids
134 clades were generally similar to or greater than vertebrate-wide %seqIDs (Figure 1 – bar graphs and
135 Table 1). In contrast, the hair cell subunits showed lower %seqIDs, with the α10 subunit depicting
136 the lowest value of all nAChR subunits (Figure 1 – bar graphs, red lines and Table 1). As previously
137 reported with smaller datasets (Franchini and Elgoyhen, 2006; Lipovsek et al., 2012), the present
138 extended analysis showed that α10 subunits are unique in presenting a segregated grouping of
139 orthologues. Thus, whereas the orthologue sequences for most nAChR subunits grouped within their
140 own respective branches, the sequences for the α10 subunits were split into two groups: non-
141 mammalian α10 subunits as a sister group to all α9 subunits, and mammalian α10 subunits an
142 outgroup to the α9/non-mammalian α10 branch (Figure 1 and Supplementary Figures 1-2). This
143 segregation reflects the great divergence of mammalian α10 amino acid sequences with respect to
144 their non-mammalian orthologues. In particular, mammalian and sauropsid sequences presented a
145 low degree of between-clade conservation compared to the other nAChR subunits (61.29% - Table
146 1). Overall, the extended molecular evolution analysis of nAChR subunits showed that while
147 neuronal subunits were highly conserved across all vertebrate clades, α10 hair cell subunits showed
148 the greatest degree of sequence divergence.

149 The capability to co-assemble into functional receptors and the co-expression of nAChR subunits
150 within a given cell delineate the complement of receptors that shape its nicotinic ACh response.
151 Numerous heterologous expression experiments and subunit-specific pharmacological studies have
152 outlined a comprehensive repertoire of functionally validated pentameric assemblies
153 (Supplementary Table 2 and references therein). However, no systematic gene expression analysis
154 that explores the potential spectrum of nAChRs in a given cell type has been performed. In order to
155 evaluate co-expression patterns, and therefore the potential for co-assembly of nAChR subunits into
156 functional receptors in different cell-types, we sourced expression data from 10 recent single-cell
157 transcriptomic studies (Supplementary Table 3). First, from the gene expression matrices we
158 identified the repertoire of nAChR subunits detected in each single cell (Supplementary Figure 3).
159 Subsequently, we used a Bayesian approach (Kharchenko et al., 2014) to estimate the likelihood of a
160 gene being expressed at any given average level in a given cell type (Supplementary Table 4), thus
161 allowing us to both compare expression levels of individual subunits across cell types (Figure 2A and
162 Supplementary Figure 4) and survey the relative expression of subunits within each cell type. We
163 next combined this data with the catalogue of validated nAChR pentamers (Supplementary Table 2)
164 and outlined the potential complement of pentameric receptors present in each cell type, by
165 identifying the subunit combinations that are present within a 10-fold, 100-fold or 1000-fold range
166 of expression level or altogether absent (Figure 2B). As expected, neurons express a range of
167 neuronal nAChR variants. Major neuronal types are identified by their well characterised nAChRs.
168 For example, visceral motor neurons from thoracic sympathetic ganglia express receptors containing
169 α3 and β4 subunits, while cortical neurons express receptors containing α4, β2 and α7 subunits.
170 Ventral midbrain dopaminergic neurons express high levels of the α6 subunit, together with β2 and
171 β3 subunits and variable levels of α3, α4 and α5 subunits (Figure 2A). Receptors containing the α2
172 subunit are almost exclusively observed in retinal neurons. Also, GABAergic, glutamatergic and
173 dopaminergic neurons from hypothalamus, ventral midbrain and/or sympathetic ganglia present
174 noticeably different potential complements of nAChRs (Figure 2B). Differences in potential nAChRs
175 composition can be observed even between closely related cell types. For example, two subtypes of
176 cortical pyramidal neurons that differ on their projection targets (Chevée et al., 2018) show a
177 significant difference in the expression level of the α5 subunit (Figure 2C), indicating they could
178 differ on the ratio of α4β2/α4α5β2 receptors on the plasma membrane. Finally, inner ear hair cells
179 co-express high levels of α9 and α10 subunits (Figure 2D).

180 Taken together the analysis of aminoacid sequences and co-expression patterns indicates that,
181 whereas the α9 and α10 subunits have a restrict expression pattern, they also have the highest

182 sequence divergence. On the contrary, neuronal nAChRs present higher sequence identity together
183 with a widespread expression pattern.

184 **Divergence of biophysical properties differentiates neuronal from hair cell nAChRs**

185 The restricted expression pattern of hair cell α9 and α10 nAChR subunits (Figure 2) and their
186 exclusive co-assembly with each other (Elgoyhen et al., 1994; Elgoyhen et al., 2001; Scheffer et al.,
187 2007; Sgard et al., 2002), together with the higher level of α10 amino acid sequence divergence
188 (Figure 1 and Table 1), indicate the potential for functional innovations across clades through
189 changes in their coding sequences. In contrast, the high conservation of neuronal subunits coding
190 sequences (Figure 1 and Table 1) may have resulted in highly conserved functional properties of
191 neuronal receptors assembled from the same subunits. We experimentally tested this prediction by
192 performing a comprehensive side-by-side comparison of the functional properties of the two main
193 neuronal, α4β2 and α7 nAChRs, and the hair cell α9α10 nAChR from three representative species of
194 tetrapod clades. To this end, we injected *Xenopus laevis* oocytes with the corresponding cRNAs and
195 characterised the biophysical properties of ACh responses.

196 *ACh evoked responses in tetrapod α4β2, α7 and α9α10 nAChRs*

197 We first evaluated the ACh apparent affinity of α4β2, α7 and α9α10 nAChRs by performing
198 concentration–response curves. Oocytes injected with rat (*Rattus norvegicus*), chicken (*Gallus gallus*)
199 or frog (*Xenopus tropicalis*) α4 and β2 cRNAs responded to ACh and showed the characteristic two-
200 component ACh dose-response curves that correspond to the well described $(\alpha4)_3(\beta2)_2$ and
201 $(\alpha4)_2(\beta2)_3$ prevalent stoichiometries (Figure 3A, Table 2 and (Moroni et al., 2006; Zwart and
202 Vijverberg, 1998)). Oocytes injected with rat, chicken or frog α7 cRNA responded to ACh with similar
203 apparent affinities (Figure 3A, Table 2 and (Couturier et al., 1990; Papke and Porter Papke, 2002)).
204 Finally, rat, chicken and frog α9 and α10 subunits formed functional heteromeric α9α10 nAChRs that
205 responded to ACh in a concentration-dependent manner (Figure 3A and (Elgoyhen et al., 2001;
206 Lipovsek et al., 2012)). The frog α9α10 receptor exhibited a significantly higher apparent affinity
207 than its amniote counterparts ($p = 0.0026$ (vs rat), $p = 0.0060$ (vs chick) – Figure 3A and Table 2).

208 It has been previously reported that rat α9 (Figure 3B and (Elgoyhen et al., 1994)) and chicken α9
209 (Figure 3B and (Lipovsek et al., 2014)) subunits can form functional homomeric receptors. Likewise,
210 frog α9 subunits assembled into functional homomeric receptors (Figure 3B). In contrast, rat α10
211 subunits cannot form functional receptors on their own (Figure 3B and (Elgoyhen et al., 2001)).
212 Surprisingly, both chicken α10 (Figure 3B and (Lipovsek et al., 2014)) and frog α10 subunits
213 assembled into functional homomeric receptors (Figure 3B).

214 In summary, α4β2 and α7 receptors from representative tetrapods showed similar responses to ACh
215 with no inter-species differences in apparent affinity. In contrast the frog α9α10 receptor exhibited a
216 10-fold difference in ACh apparent affinity compared to its amniote counterparts. Finally, α10
217 subunits showed clade-specific differences in the ability to form functional homomeric receptors in
218 the oocyte heterologous expression system.

219 *Desensitization profiles of tetrapod α4β2, α7 and α9α10 nAChRs*

220 A defining feature of nAChRs is their desensitisation upon prolonged exposure to the agonist (Quick
221 and Lester, 2002). Rat and chicken neuronal α4β2 receptors are characterised by slow
222 desensitisation kinetics (Mazzaferro et al., 2017). As shown in Figure 4, 70-80% of the maximum
223 current amplitude remained 20 seconds after the peak response to 100 µM ACh. Similarly, frog α4β2
224 receptors depicted slow desensitisation profiles, with no significant differences in the percentage of
225 current remaining 20 seconds after the peak response to 100 µM ACh when compared to that of rat
226 ($p = 0.7326$ – Table 2) and chicken α4β2 ($p = 0.7204$ – Table 2) nAChRs (Figure 4). The frog α7
227 nAChRs showed fast desensitisation with 2-3% of current remaining 5 seconds after the peak
228 response to 1 mM ACh, similar to that of rat α7 ($p = 0.3743$ – Table 2) and chicken α7 ($p = 0.2496$ –
229 Table 2) nAChRs (Figure 4 and (Bouzat et al., 2017; Couturier et al., 1990)).

230 The conserved desensitisation profiles observed for both types of neuronal receptors was in stark
231 contrast with that of α9α10 receptors (Figure 4 and Table 2). While rat and chicken α9α10 receptors
232 showed similar and somewhat slow desensitization, with 60-65% of current remaining 20 seconds
233 after the peak response to ACh ($p = 0.9999$ – Table 2), frog α9α10 nAChRs exhibited significantly
234 higher desensitization (14.5% of current remaining 20 seconds after the ACh peak) when compared
235 to rat α9α10 ($p=0.0051$ – Table 2) and chicken α9α10 ($p=0.0042$ – Table 2) receptors.

236 *Modulation by extracellular calcium of tetrapod α4β2, α7 and α9α10 nAChRs*

237 Neuronal nAChRs are potentiated by extracellular divalent cations such as Ca^{2+} via an allosteric and
238 voltage-independent mechanism (Galzi et al., 1996; Mulle et al., 1992; Vernino et al., 1992). The rat
239 α9α10 nAChR, on the other hand, is both potentiated and blocked by physiological concentrations of
240 extracellular divalent cations (Weisstaub et al., 2002). Blockage occurs in the micromolar range, is
241 voltage dependent and proposed to occur as a result of calcium permeation (Weisstaub et al., 2002).
242 To perform a comparative analysis of calcium modulation on rat, chicken and frog α4β2, α7 and
243 α9α10 receptors, responses to near-EC_{50} concentrations of ACh were recorded in normal Ringer's
244 solution at a range of Ca^{2+} concentrations and normalised to the response at 1.8 mM Ca^{2+} (Figure 5).
245 For the neuronal α4β2 (Figure 5 - top panels) and α7 (Figure 5 - middle panels) receptors from all
246 three species, a similar potentiation pattern was observed, with increasingly higher responses to

247 ACh at greater Ca^{2+} concentrations. In contrast, responses of α9α10 nAChRs from rat, chicken and
248 frog (Figure 5 - bottom panels) exhibited differential modulation by extracellular Ca^{2+}. As previously
249 reported for the rat α9α10 receptor, responses to ACh were potentiated by extracellular Ca^{2+}, with
250 maximal responses observed at 0.5 mM. Higher Ca^{2+} concentrations resulted in block of ACh
251 responses (Figure 5 - bottom left panel and Weisstaub et al., 2002). The chicken α9α10 receptor also
252 showed peak potentiation of the ACh response at 0.5 mM extracellular Ca^{2+}. However, no evident
253 block was observed at higher concentrations of the cation (Figure 5 - bottom middle panel). Finally,
254 the frog α9α10 receptor showed potentiation of ACh responses at all Ca^{2+} concentrations assayed,
255 with maximal responses detected at 3 mM Ca^{2+} (Figure 5 - bottom right panel). In summary, α4β2
256 and α7 neuronal receptors showed no significant inter-species differences in modulation by
257 extracellular calcium. In contrast, α9α10 receptors showed species specific features, with frog α9α10
258 receptors showing a calcium modulation profile similar to that of neuronal receptors.

259 *Calcium permeability of tetrapod α4β2, α7 and α9α10 nAChRs*

260 Calcium permeation through nAChRs holds great functional significance for the activation of calcium
261 dependent conductances and intracellular signalling pathways (Dani and Bertrand, 2007). Receptors
262 containing the α7 subunit have high calcium permeability (Séguéla et al., 1993) whereas receptors
263 containing α4β2 subunits have a lower contribution of calcium to the total current (Haghighi and
264 Cooper, 2000; Lipovsek et al., 2012). Inner ear hair cell α9α10 nAChRs are unique in their inhibitory
265 synaptic activity via calcium dependent coupling to SK2 channels in mammals (Glowatzki and Fuchs,
266 2000; Goutman et al., 2005), birds (Fuchs and Murrow, 1992a; Fuchs and Murrow, 1992b), turtles
267 (Art et al., 1984) and frogs (Castellano-Muñoz et al., 2010). Differences in calcium permeability
268 between mammalian and avian α9α10 nAChRs have been reported and proposed to be linked to a
269 differential role of intracellular calcium stores in efferent modulation of hair cell activity and the
270 mammalian specific coupling to BK channels (Lipovsek et al., 2014; Lipovsek et al., 2012).

271 In order to perform a comparative analysis of the extent of the calcium component of ACh responses
272 of tetrapod neuronal and hair cell nAChRs, we studied the differential activation of the oocyte's
273 endogenous calcium-activated chloride current (ICl_{Ca}). In oocytes expressing a recombinant receptor
274 with high calcium permeability, the ICl_{Ca} is strongly activated upon ACh application (Barish, 1983;
275 Miledi and Parker, 1984). Incubation of oocytes with the membrane-permeant fast Ca^{2+} chelator
276 BAPTA-AM subsequently abolishes the Cl^- component of the total measured current (Gerzanich et
277 al., 1994). Figure 6 shows representative responses to ACh before and after a 3-hour incubation with
278 BAPTA-AM for α4β2, α7 and α9α10 nAChRs from rat, chicken and frog. Whereas ACh-evoked
279 currents were only slightly affected in all α4β2 nAChRs denoting no major calcium influx (70-80% of

280 current remaining after BAPTA incubation, Figure 6, left panels), all α7 receptors showed a strong
281 reduction of the ACh response after BAPTA incubation (30-40% of current remaining after BAPTA),
282 indicating significant calcium permeation (Figure 6, middle panels). Thus, no inter-species
283 differences in the proportion of calcium current for both the low calcium permeant α4β2 and the
284 highly calcium permeant α7 neuronal receptors were observed (Table 2). Conversely, and as
285 previously reported (Lipovsek et al., 2014; Lipovsek et al., 2012), we observed a marked difference in
286 the extent of calcium current between the rat and chicken α9α10 receptors ($p = 0.0299$ – Figure 6,
287 right panels and Table 2). Moreover, the percentage of remaining response after BAPTA-AM
288 incubation for the frog α9α10 receptor (Figure 6, right panels) was similar to that of the rat receptor
289 ($p = 0.9999$ – Table 2) and significantly different from that of the chicken α9α10 nAChR ($p = 0.0013$ –
290 Table 2). In summary, while α7 and α4β2 neuronal nAChRs showed no inter-species difference in the
291 extent of calcium current, the frog α9α10 receptor showed a calcium component significantly higher
292 than that of its chicken counterpart and similar to that of the rat α9α10 receptor.

293 *Current-voltage relationships of tetrapod α4β2, α7 and α9α10 nAChRs*

294 Neuronal nAChRs are characterised by a strong inward rectification, with negligible current at
295 depolarized potentials (Bertrand et al., 2006; Sands and Barish, 1992; Séguéla et al., 1993). This is
296 proposed to be a relevant feature for their roles as pre-synaptic modulators of neuronal
297 transmission (Haghighi and Cooper, 2000). On the other hand, amniote α9α10 nAChRs exhibit a
298 peculiar current-voltage (I-V) relationship due to a considerable outward current at positive
299 potentials (Elgoyhen et al., 2001; Lipovsek et al., 2012).

300 In order to perform a comparative analysis of the rectification profiles of neuronal and hair cell
301 nAChRs we obtained I-V curves by applying a 2 seconds voltage ramp protocol (-120 to +50 mV) at
302 the plateau of ACh response for α4β2 and α9α10 nAChRs or by recording the current amplitude
303 elicited by 100 μM ACh at different holding potentials for the highly desensitizing α7 receptor. All
304 neuronal nAChRs exhibited I-V curves with marked inward rectification with no significant inter-
305 species differences for either α4β2 or α7 tetrapod receptors (Figure 7, top left and middle panels
306 and Table 2). Conversely, each of the hair cell α9α10 nAChRs analysed presented its unique I-V
307 profile. As previously reported, rat α9α10 receptors showed significant outward current at
308 depolarised potentials and greater inward current at hyperpolarised potentials (Figure 7, top right
309 panel and Elgoyhen et al., 2001). The chicken α9α10 receptor showed outward current similar to
310 that of the rat α9α10 receptor, but the inward current was smaller (Figure 7, top right panel).
311 Surprisingly, the frog α9α10 receptor showed an I-V profile similar to that of neuronal nAChRs, with
312 strong inward rectification and almost no outward current at depolarised potentials (Figure 7). In

313 order to quantify the degree of rectification exhibited by each nAChR subtype we obtained the ratio
314 of current at +40 mV to that at -90 mV (I_{+40}/I_{-90}, Figure 7, bottom panels). Neuronal nAChRs
315 presented I_{+40}/I_{-90} values smaller than 1, denoting their pronounced inward rectification and showing
316 no inter-species differences (Table 2). In contrast, the I_{+40}/I_{-90} ratio of α9α10 receptors reflected the
317 differences in rectification profile (Table 2), with the frog α9α10 receptor showing a I_{+40}/I_{-90} below 1
318 and significantly different to the higher values obtained for the chick α9α10 ($p = 0.0406$ – Table 2)
319 and rat α9α10 ($p < 0.0001$ – Table 2) receptors that also differed between each other ($p = 0.0229$ –
320 Table 2). In summary, while neuronal α4β2 and α7 receptors showed no interspecies differences, the
321 α9α10 receptors from the three species analysed showed their own individual I-V curves with
322 different patterns and degrees of rectification.

323 **Comparative functional analysis of neuronal and hair cell nAChRs shows distinct evolutionary**
324 **trajectories**

325 Altogether, the characterisation of individual functional properties of tetrapod nAChRs showed a
326 stark contrast between neuronal and hair cell nAChRs. In order to concomitantly analyse the
327 diversification, or conservation of receptor function, we performed principal component analysis
328 (PCA) on all the functional variables measured on α4β2, α7 and α9α10 receptors from the three
329 species (Table 3). The first two principal components accounted for 82% of the variability (Figure 8).
330 Moreover, the distribution of receptors in PCA space reflected their overall functional differences
331 and similarities. Both neuronal α4β2 and α7 receptors occupied distinct regions, more distant in PC1
332 than in PC2 denoting that these receptors differ more on ACh apparent affinity, desensitisation and
333 calcium permeability than they do on rectification and calcium modulation (Figure 8). Also, α4β2 and
334 α7 receptors from the different species were located very close together, reflecting the lack of inter-
335 species differences in functional properties. In contrast, the hair cell α9α10 receptors from the
336 different species were distant from each other in PCA space, denoting their extensive functional
337 divergence (Figure 8). Interestingly, the frog α9α10 nAChR was closer to the α7 receptors than to its
338 amniote counterparts, highlighting the overall functional similarity between the amphibian α9α10
339 and α7 nAChRs.

340 Amino acid sequence phylogenies, co-expression/co-assembly patterns and functional experiments
341 support the hypothesis of differential evolutionary trajectories for neuronal and hair cell receptors.
342 Further insight could be attained by the evaluation of these parameters on the receptors present in
343 the last common ancestor of rat and chicken (amniote ancestor) and of rat, chicken and frog
344 (tetrapod ancestor). To tackle this, we inferred amniote and tetrapod ancestral sequences for the
345 receptors and predicted the character state for the functional properties on the α4β2, α7 and α9α10

346 ancestral receptors (see methods). We then projected this predicted functional states onto the
347 functional PCA space of the extant receptors (Figure 8). As expected, the predicted ancestral α4β2
348 and α7 amniote and tetrapod receptors were located close to their extant counterparts. In contrast,
349 the predicted ancestral states of the α9α10 receptors were localised halfway between the frog
350 α9α10 and the amniote chicken and rat α9α10 extant receptors, potentially reflecting the functional
351 evolutionary trajectory of the hair cell receptor. Thus, the ancestral tetrapod α9α10 receptor may
352 have functionally resembled the extant frog α9α10 receptor and neuronal α7 receptors, mainly on
353 properties with heavier loading on PC2 (i.e., rectification and calcium permeability). Moreover, the
354 ancestral amniote α9α10 receptor may have had functional properties that more closely resembled
355 those of neuronal α4β2 receptors, in particular for properties with heavier loading on PC1 (i.e., ACh
356 apparent affinity, desensitization and calcium modulation). In summary, the data portrayed in Figure
357 8, that incorporates information on amino acid sequence and functional properties, describes a
358 plausible scenario for the functional evolutionary trajectories undertaken by two neuronal and the
359 hair cell nAChRs within the tetrapod lineage.

360

361 **Discussion**

362 The expansion of ion channel families on the vertebrate stem branch was mostly driven by the two
363 rounds of whole genome duplications (Roux et al., 2017). This has played a crucial role in the
364 evolution of nervous systems and provided raw material that enabled the diversification of cell types
365 (Liebeskind et al., 2015) resulting in the complexity acquired by vertebrate brains (e.g.(Sugino et al.,
366 2019)). Among the different ion channel families, Cys-loop receptors are within those that
367 underwent the greatest expansion (Liebeskind et al., 2015). While the last common ancestor to
368 bilateria most likely had at least an α7-like subunit, an α9-like, a neuronal/muscle α-like and a
369 neuronal/muscle β-like subunit (Dent, 2006), the entire extant complement of nAChRs, which
370 includes 17 different subunits (α1-α10, β1-β4, δ, ε and γ), was already present in the last common
371 ancestor of all vertebrates (Pedersen et al., 2019). With the exception of some fish species that
372 acquired α11, β1.2 and β5 subunits, for which no expression or functional data has yet been
373 reported (Pedersen et al., 2019), and the loss of the α7-like α8 subunits in mammals, the
374 complement of original vertebrate nAChR subunits has been remarkably conserved. Moreover,
375 within the repertoire of ligand-gated ion channels, nAChRs are unique in that distinct members of
376 the family have non-overlapping and segregated roles in synaptic transmission, either in the nervous
377 system, inner ear hair cells or the neuromuscular junction (Dani and Bertrand, 2007; Elgoyhen and
378 Katz, 2012; Mishina et al., 1986). In this work, we performed in-depth analyses of coding sequence
379 phylogeny, subunit co-expression patterns and comparative functional properties of neuronal and
380 hair cell receptors to explore the potential impact of these segregation of nAChRs subgroups on their
381 respective evolutionary histories. We found a stark contrast between neuronal and hair cell
382 receptors in all variables analysed. Neuronal subunits showed high degree of coding sequence
383 conservation, coupled to greater co-expression variability and conservation of functional properties
384 across tetrapod clades. In contrast, the hair cell α9α10 nAChR showed greater sequence divergence,
385 a highly restricted co-expression pattern and a great degree of variability of functional properties
386 across species. These results indicate that along the tetrapod lineage neuronal and hair cell nAChRs
387 underwent alternative evolutionary trajectories. These were most likely shaped by the differential
388 availability of substrates on which random changes and selection pressure could act upon that
389 resulted from the segregating co-expression patterns and co-assembly rules of component subunits.

390 The observation that the biophysical functional properties of α4β2 and α7, as examples of neuronal
391 nAChRs, were conserved in the three tetrapod species analysed, relates to their high degree of
392 amino acid sequence conservation (Figure 1 and Table 1). Cholinergic innervation is pervasive, with
393 almost every area of the brain being influenced by nicotinic signalling (Dani and Bertrand, 2007).
394 Moreover, the expression of nAChR subunits is extremely widespread in the central and peripheral

395 nervous system and neuronal nAChRs assemble in multiple combinations (Supplementary Table 2).
396 Thus, randomly acquired changes in the coding sequence of a given subunit might be deleterious for
397 receptor function in a multitude of neuronal types. Such coding sequence changes would therefore
398 be under strong negative selection pressure. This is in agreement with the absence of signatures of
399 positive selection in the protein-coding DNA sequences of α4, β2 and α7 subunits (Lipovsek et al.,
400 2012). Moreover, it parallels previous reports showing that the coding regions of brain expressed
401 genes show little or no evidence of positive selection (Haygood et al., 2010; Nielsen et al., 2005).

402 The strong conservation of coding sequence and functional properties we describe here for neuronal
403 nAChRs, most likely due to negative selection pressure, excludes this substrate as a potential source
404 of random change that could subsequently result in functional diversification. However, variability in
405 neurons could alternatively result from a re-shuffling of the complement of nAChR subunits being
406 expressed. Therefore, and as for most brain expressed genes (Haygood et al., 2010; He et al., 2017;
407 Hoekstra and Coyne, 2007; Meyer et al., 2017; Nielsen et al., 2005), random changes in non-coding
408 regions that lead to differential expression patterns across brain areas or species may have played a
409 substantial role in delineating the evolutionary trajectories of these subtype of nAChRs. Thus, the
410 differential expression of neuronal nAChRs in different neuronal types, together with the multiple
411 alternative heteropentameric assemblies (Supplementary Table 2 and (Zoli et al., 2015)), are the
412 most likely pool of diversity potential. Functional neuronal receptors can be assembled from single α
413 subunits (e.g. α7), single α and single β subunits (e.g. α4β2), multiple α subunits with single β
414 subunits (e.g. α4α5β2), single α and multiple β subunits (e.g. α6β3β4) and multiple α and β subunits
415 (e.g. α4α5β2β3) (Supplementary Table 2 and references therein). Diversity of neuronal nAChRs is
416 further expanded via the assembly of alternative stoichiometries (e.g. $\alpha4_2\beta2_3$ and $\alpha4_3\beta2_2$). In
417 agreement with this, our survey of expression patterns across the mouse brain provides numerous
418 instances of potential functional variability and diversification, even between closely related
419 neuronal types. For example, dopamine exerts a key role in motivation and reinforcement (Schultz,
420 2007; Waelti et al., 2001) and this is known to be involved in the addictive properties of nicotine
421 (Picciotto and Corrigall, 2002; Picciotto et al., 1998). The differential co-expression patterns of
422 nAChR subunits between the four different subtypes of dopaminergic (DA) midbrain ventral
423 tegmental area (VTA) neurons defined by transcriptomic analysis ((La Manno et al., 2016) and Figure
424 2) may contribute to the understanding of the differential control of dopaminergic neuron-firing
425 patterns by cholinergic input (Mameli-Engvall et al., 2006; Maskos et al., 2005). The α4 and β2
426 subunits can co-assemble with α5 or β3 subunits (Jain et al., 2016; Kuryatov et al., 2008; Ramirez-
427 Latorre et al., 1996). Inclusion of α5 can alter α4β2* nicotinic receptor properties substantially,
428 increasing ACh sensitivity, desensitization kinetics and Ca^{2+} permeability (Kuryatov et al., 2008;

429 Ramirez-Latorre et al., 1996; Tapia et al., 2007). In addition, incorporation of the β3 subunit to the
430 α4β2* receptor also increases ACh sensitivity, without significantly affecting Ca^{2+} permeability
431 (Kuryatov et al., 2008; Tapia et al., 2007). While the β2 and β3 subunits are expressed at comparable
432 levels in all four VTA DA neuron types, VTA2 and VTA4 showed lower levels of α4, and α5 expression
433 was present at different (albeit low levels) in VTA1, VTA2 and VTA4 and absent in VTA3 DA neurons.
434 This indicates that the four subtypes of DA neurons might express differential levels of functionally
435 distinct α4β2, α4α5β2 and α4β2β3 receptors. Moreover, they all showed equally high levels of the
436 α6 subunit and low (or undetectable) levels of the α3 subunit, both of which can co-assemble with
437 α4, α5 and/or β2 subunits, greatly enhancing the complexity of individual nAChRs-mediated
438 responses of VTA DA neurons to modulatory cholinergic input.

439 Cortical pyramidal neurons provide a further example of the incremental value of transcriptomic
440 analysis of the complement of nicotinic subunits. The activity of cortical layer VI neurons is
441 modulated by a dense cholinergic innervation from the basal forebrain and ACh elicits robust
442 excitatory responses acting on α4β2* nAChRs. Moreover, layer VI is one of the few cortical areas
443 that express the accessory α5 nAChR subunit (Proulx et al., 2014; Tian et al., 2014). Cortical neurons
444 that project to both the ventral posteromedial nucleus (VPM) and the posteromedial complex of the
445 thalamus express significantly higher levels of the α5 subunit than neurons projecting to the VPM
446 only (Figure 2C). This suggests VPM-only projecting neurons could have a lower density of α4α5β2
447 compared to α4β2 nAChRs. In turn, this may contribute to differential cholinergic modulation of
448 these subtypes of layer VI neurons, that also show differences in excitability (Landisman and
449 Connors, 2007).

450 The widespread and overlapping expression of neuronal nAChR subunits is in sharp contrast with the
451 extremely narrow expression pattern of α9 and α10 subunits. As expected, these are only co-
452 expressed at very high levels in inner ear hair cells (Figure 2D). With the exception of trace levels of
453 α10 (not accompanied by α9) at some hypothalamic neurons, hair cell subunits are not expressed in
454 the brain areas surveyed. These observations support the notion that α9 and α10 are not a subtype
455 of brain nicotinic subunits (for reviews see (Morley et al., 2018)), but form a group of their own,
456 characterised by unique expression profile, pharmacological and biophysical properties (Elgoyhen et
457 al., 1994; Elgoyhen et al., 2001; Katz et al., 2000; Weisstaub et al., 2002). Most notably, nicotine, the
458 diagnostic agonist of the nAChRs family, does not act as an agonist of α9α10 receptors, but as a
459 competitive antagonist (Elgoyhen et al., 2001). This is in line with the vast body of literature
460 indicating that α9α10 nAChRs exclusively mediate fast efferent neurotransmission to cochlear and
461 vestibular hair cells in the inner ear (Elgoyhen et al., 1994; Elgoyhen and Katz, 2012; Elgoyhen et al.,
462 2001; Holt et al., 2001; Parks et al., 2017).

463 In addition to high levels of α9 and α10 subunits, hair cells express a number of neuronal (β2 and β4)
464 and muscle (α1, β1, γ/ε) subunits (Figure 2 and (Roux et al., 2016; Scheffer et al., 2007)). However,
465 no responses to nicotine application are detected in hair cells (Fuchs and Murrow, 1992b; Gomez-
466 Casati et al., 2005; Scheffer et al., 2007), indicating that functional muscle or neuronal nAChRs are
467 not present at the plasma membrane. The detection of neuronal and muscle subunits mRNA may
468 result from redundant or residual transcription regulation mechanisms. In that context, developing
469 hair cells appear to recapitulate the γ to ε switch in accessory muscle subunit expression (Figure 2A)
470 that characterises neuromuscular junction maturation (Mishina et al., 1986). Moreover, similar
471 "leaky" expression of muscle subunits was detected in a number of neuronal types (Figure 2A).Of
472 note, muscle subunits showed relatively low levels of coding sequence conservation (Figure 1).
473 However, muscle cells can toggle between at least two receptor variants (Mishina et al., 1986).
474 These observations place muscle receptors in between the two extremes of hair cell (isolated) and
475 neuronal (widespread) receptors. Then, a further test of our hypothesis would be to perform a
476 comparative study of muscle receptors, with the prediction that a modest level of functional
477 divergence may be encountered, but outperformed by the differences between muscle receptor
478 variants.

479 Spiral ganglion neurons provide afferent innervation to cochlear hair cells and express a range of
480 neuronal nAChR subunits (Figure 2 and (Hiel et al., 1996; Morley et al., 1998; Reijntjes and Pyott,
481 2016)). Interestingly, low levels of α9 and α10 subunits are present in SGNs (Figure 2 and (Shrestha
482 et al., 2018)) and similarly low expression was detected by two other independent single-cell RNA
483 sequencing studies (Petitpre et al., 2018; Sun et al., 2018). If this low level of α9 and α10 mRNA
484 proves to be more than "transcriptional noise" then SGNs may be unique among neurons in
485 expressing the hair cell α9α10 receptor. This might be related to the shared developmental origin of
486 SGNs and HCs at the otic placode (Arendt et al., 2016; Fritzsch and Beisel, 2004) and could open the
487 possibility that in addition to neuronal nAChRs, which are thought to partly mediate the nicotinic
488 effect of lateral olivocochlear terminals on afferent dendrites (Reijntjes and Pyott, 2016), α9α10
489 nAChRs may also play a role. Finally, α9 expression was not detected in any dorsal root ganglion
490 neurons, while α10 is present at very low levels in only a few subtypes (Figure 2A and (Usoskin et al.,
491 2015)). These observations support those reported by qPCR and functional assays (Hone et al., 2011;
492 Rau et al., 2004) and provide further evidence that the participation of α9* nAChRs in pain processes
493 is not due to its presence in DRG neurons (Hone et al., 2011; Rau et al., 2004).

494 The observations that α9 and α10 genes are only co-ordinately transcribed at inner ear hair cells,
495 together with their ability to only form functional heteromeric receptors when co-assembled with
496 each other but not with other nAChR subunits (Elgoyhen et al., 1994; Elgoyhen et al., 2001; Scheffer

497 et al., 2007), support our hypothesis that evolutionary changes in the hair cell receptors may have
498 been focused at the coding sequence. Moreover, it suggests that species specific differences in
499 olivocochlear cholinergic synaptic transmission could only rely upon modifications in the functional
500 properties of α9α10 nAChRs. Accordingly, vertebrate α9 and α10 subunits exhibit low overall amino
501 acid sequence identity (Table 1 and Figure 1), with mammalian α10 subunits showing a higher than
502 expected accumulation of non-synonymous substitutions that were positively selected (Franchini
503 and Elgoyhen, 2006; Lipovsek et al., 2012). In addition, α9 subunits also show a high number of
504 mammalian-specific changes (Lipovsek et al., 2014). As a consequence of this evolutionary
505 trajectory, the biophysical properties of α9α10 receptors drastically changed across vertebrate
506 species (Figure 8 and (Lipovsek et al., 2014; Lipovsek et al., 2012)). Crucially, given the restricted
507 expression pattern and the exclusive co-assembly of the α9 and α10 subunits, these were isolated
508 evolutionary events within the nAChRs family that did not alter cholinergic synaptic function in other
509 cell types.

510 Of note, α9 and α10 expression, together with other nAChR subunits, has been reported in other
511 peripheral, non-neuronal, tissues (McIntosh et al., 2009; Zoli et al., 2018). For example, several
512 immune, skin, bladder urothelial and nasal non-neuronal epithelial cells express a number of
513 nicotinic and muscarinic cholinergic receptor subunits (Hao et al., 2011; Keiger et al., 2003; Kurzen et
514 al., 2007; McIntosh et al., 2009; Sato et al., 1999; Zarghooni et al., 2007). Therefore a plausible
515 autocrine/paracrine effect of ACh in these cells can be served by a multiple and redundant battery of
516 nAChRs that might play a metabotropic function in these peripheral tissues (Criado, 2018;
517 Zakrzewicz et al., 2017). Due to the redundancy in pathways for ACh signalling, it is unlikely that the
518 function of α9α10 nAChRs in these peripheral tissues provided the selection forces that shaped the
519 accumulation of non-synonymous changes on this receptor. Moreover, if these were the case, a
520 similar process could be predicted for neuronal nAChRs expressed in these cells, an event that did
521 not occur since neuronal nAChR subunits are under strong purifying selection (Lipovsek et al., 2012).

522 The comparative analysis of functional properties of α9α10 nAChRs from representative tetrapods
523 showed unprecedented divergence (summarised in Figure 8). Since the primary function of the
524 α9α10 receptor is at the postsynaptic side of the efferent modulation of hair cell activity, it can be
525 hypothesised that the evolutionary changes in receptor function may be coupled to the evolutionary
526 processes undertaken by the inner ears of the different clades. Upon the transition to land, the
527 hearing organs of tetrapods underwent parallel evolutionary processes, mainly due to the
528 independent emergence of the tympanic middle ear, at least five times, in separate groups of
529 amniotes (Manley, 2017; Tucker, 2017). This was followed by the independent elongation of the
530 auditory sensory epithelia that extended the hearing range to higher frequencies and the

531 elaboration of passive and active sound amplification mechanisms that lead to the fine tuning of
532 sound detection (Dallos, 2008; Hudspeth, 2008; Manley, 2017). More importantly, mammals and
533 sauropsids underwent a parallel diversification of hair cell types, segregating, partially in birds but
534 completely in mammals, the phonoreception and sound amplification functions (Koppl, 2011).
535 Efferent innervation to hair cells, mediated by α9α10 nAChRs, is an ancestral feature common to all
536 vertebrate species (Sienknecht et al., 2014). In the auditory epithelia it modulates sound
537 amplification and followed the hair cell diversification pattern: in birds it mainly targets short hair
538 cells, while in mammals it targets outer hair cells (Koppl, 2011). The latter developed a clade-specific
539 sound amplification mechanism that is brought about by the motor protein prestin, through a
540 process known as somatic electromotility (Oliver et al., 2001). Prestin, together with βV giant
541 spectrin, a major component of the outer hair cells' cortical cytoskeleton which is necessary for
542 electromotility and the voltage-gated potassium channel gene KCNQ4 all show signatures of positive
543 selection in the mammalian clade that may relate to the acquisition of somatic electromotility
544 (Cortese et al., 2017; Franchini and Elgoyhen, 2006; Liu et al., 2012). Thus, the mammalian clade-
545 specific evolutionary processes observed in both the α9 and α10 subunits (Franchini and Elgoyhen,
546 2006; Lipovsek et al., 2014; Lipovsek et al., 2012) may be related to overall changes in the efferent
547 olivovochlear systems of this clade that is tasked with the modulation of prestin-driven somatic
548 electromotility. A recent high throughput evolutionary analysis identified 167 inner ear expressed
549 genes with signatures of positive selection in the mammalian lineage (Pisciottano et al., 2019). Thus,
550 genes expressed in the inner ear can be considered as hotspots for evolutionary innovation in the
551 auditory system across species, a process that appears to have particularly affected the α9α10
552 nAChR. In such a scenario, the inter-species differences in the extent of calcium current provide a
553 context for evaluating the relationship between evolutionary trajectories and the functional role of
554 α9α10 receptors. In mammals, the high calcium influx through α9α10 receptors activates large
555 conductance, voltage and low-calcium-sensitive BK potassium channels mediating hyperpolarization
556 of outer hair cells in higher frequency regions of the cochlea (Wersinger et al., 2010). In contrast, in
557 short hair cells from the chicken basilar papillae, hyperpolarization is served by the ACh-dependent
558 activation of high calcium sensitive SK potassium channels (Fuchs and Murrow, 1992a; Fuchs and
559 Murrow, 1992b; Samaranayake et al., 2004). Moreover, in contrast to adult mammalian hair cells
560 where efferent fibres directly contact outer hair cells, but not the inner hair cells that release
561 glutamate to activate afferent auditory fibres, efferent innervation in birds and amphibians co-exists
562 with afferent innervation in the same hair cells. Calcium influx in these hair cells could therefore
563 result in efferent-triggered, ACh-mediated release of glutamate to auditory afferents due to calcium
564 spill over, bypassing sound mechanotransduction. Thus, limiting the extent of calcium influx through

565 α9α10 nAChRs may be paramount to avoid confounding sensory inputs. In this hypothetical
566 scenario, the low calcium permeability of the avian α9α10 nAChR or the very high desensitization
567 kinetics of the amphibian α9α10 nAChR that restrict calcium load could be related to the
568 aforementioned selection pressure.

569 In summary, the present work provides evidence supporting different evolutionary trajectories for
570 neuronal and hair cell nAChRs. These may have resulted from the differential substrates for random
571 change that dominated evolutionary processes in each receptor subgroup: co-expression/co-
572 assembly patterns for neuronal subunits, changes in coding sequence for hair cell subunits. It results
573 salient that among ligand-gated ion channels these alternative evolutionary trajectories are a
574 particular feature of the nAChRs family of Cys-loop receptors. Thus, this is not observed for
575 ionotropic glutamate and $GABA_A$ receptors, whose 18 (Traynelis et al., 2010) and 19 (Tsang et al.,
576 2007) member subunits, respectively, are all expressed in the central nervous system. Finally, this
577 work highlights the significance of studies that traverse organisational levels. By simultaneously
578 analysing coding sequences, expression patterns and protein functional properties we were able to
579 gain new insights into the evolutionary history of gene paralogous, thus providing further context for
580 the role of nAChRs in neuronal and hair cell synaptic transmission.

581

582 **Methods**

583 All experimental protocols were carried out in accordance with the guides for the care and use of
584 laboratory animals of the National Institutes of Health and the Institutional Animal Care and Use
585 Committee of the Instituto de Investigaciones en Ingeniería Genética y Biología Molecular, "Dr.
586 Héctor N. Torres".

587 **Phylogenetic analysis of vertebrate nAChRs subunits**

588 All sequences were downloaded from GenBank (www.ncbi.nlm.nih.gov/genbank), UCSC
589 (http://genome.ucsc.edu/) and Ensembl (www.ensembl.org) databases. The signal peptides of all
590 sequences were excluded from the analysis since they are not present in the mature functional
591 protein. Accession numbers are listed in Supplementary Table 1. All sequences were visually
592 inspected, and missing and/or incorrect exons were obtained from the NCBI Genome Project traces
593 database (http://blast.ncbi.nlm.nih.gov/Blast.cgi). Sequence alignment was performed using
594 *Clustal*W on the MEGA7 software (www.megasoftware.net; (Kumar et al., 2016)), with the following
595 parameters: for pairwise alignments, gap opening penalty: 10, gap extension penalty: 0.1; for
596 multiple alignments, gap opening penalty: 10, gap extension penalty: 0.2. Protein weight matrix:
597 Gonnet. Residue specific and hydrophilic penalties: ON. Gap separation distance: 4. End gap
598 separation: OFF and no negative matrix was used. The delay divergent cutoff was 30%. The full
599 alignment for the nicotinic subunits from representative vertebrate species is available in
600 Supplementary File 1 in fasta format.

601 Average percentage sequence identity was calculated for each subunit using the percentage of
602 sequence identity between each pair of sequences from the same category for all sequences and for
603 within or between mammalian and/or sauropsid sequences. For of α10 subunits, the average
604 percentage of sequence identity was also calculated for the non-mammalian paraphyletic group.
605 Values obtained are in Table 1.

606 The phylogenetic tree of all nAChR subunits was built using the MEGA7 software. Positions
607 containing alignment gaps and missing data were eliminated only in pairwise sequence comparisons.
608 The final dataset contained a total of 773 positions. The evolutionary distances (i.e., number of
609 amino acid substitutions per site) were computed using the JTT matrix-based method (Jones et al.,
610 1992). The neighbour-joining algorithm (Saitou and Nei, 1987) was used to generate the initial tree
611 and branch support was obtained by bootstrap test (1000 replicates) (Felsenstein, 1985). The
612 evolutionary history was inferred using the minimum evolution method (Rzhetsky and Nei, 1992). A
613 first tree was generated with variation rate among sites modelled by a gamma distribution

614 (Supplementary Figure 1) and a second tree assuming uniform variation rates among sites
615 (Supplementary Figure 2). Overall, tree topology was similar between both methods.

616 **Analysis of nAChR subunit expression in single-cell RNAseq (scRNAseq) datasets**

617 Processed gene expression data tables were obtained from 10 scRNAseq studies that evaluated gene
618 expression in retina (Shekhar et al., 2016) inner ear sensory epithelium (Burns et al., 2015; McInturff
619 et al., 2018) and spiral ganglion (Shrestha et al., 2018), ventral midbrain (La Manno et al., 2016),
620 hippocampus (Cembrowski et al., 2018), cortex (Chevée et al., 2018), hypothalamus (Romanov et al.,
621 2017), visceral motor neurons (Furlan et al., 2016) and dorsal root ganglia (Usoskin et al., 2015).
622 Accession numbers, cell types inferred and number of cells analysed are summarised in
623 supplementary table 3. For all datasets, we used the published gene expression quantification and
624 cell type labels. Each dataset was analysed separately. For the retina dataset we used the Smart-
625 Seq2 sequencing data from Vsx2-GFP positive cells (Shekhar et al., 2016). For the gene expression
626 quantification we only analysed four cell types that had a minimum number of cells in the dataset
627 that allowed reliable fitting to the error models: BC1A, BC5A, BC6 and RBC. From the layer VI
628 somatosensory cortex dataset (Cembrowski et al., 2018) we used a subset of the expression matrix
629 that corresponds to day 0 (i.e. control, undisturbed neurons) of their experimental manipulation. For
630 the hypothalamic neurons dataset (Romanov et al., 2017) we used a subset that contained only
631 neurons from untreated (control) mice and only quantified gene expression on the 10 broad cell
632 types identified. From the ventral midbrain dopaminergic neurons dataset (La Manno et al., 2016)
633 we used a subset comprising DAT1-Cre/tdTomato positive neurons from P28 mice. For the SGNs
634 dataset we used a subset comprising Type I neurons from wild type mice (Shrestha et al., 2018). For
635 the utricle hair cell datasets we used the normalised expression data of (McInturff et al., 2018). For
636 the cochlear hair cell data we used the normalised expression data from (Burns et al., 2015) and
637 continued our analysis with only the 10 cochlear hair cells identified. For the visceral motor neurons
638 dataset (Furlan et al., 2016) we excluded the neurons that were "unclassified" from further analysis.
639 For the dorsal root ganglia dataset (Usoskin et al., 2015) we used a subset containing only
640 successfully classified neurons that were collected at room temperature. Inspection of al datasets for
641 batch effects and violin plots of the single cell expression of nAChR subunits (Supplementary Figure
642 3) were performed using the *scater* package (version 1.10.1) (McCarthy et al., 2017). All data analysis
643 was implemented in R (version 3.5.1) and Bioconductor (version 3.8)
644 (http://www.bioconductor.org/), running on RStudio (version 1.1.456) (http://www.rstudio.com/).

645 The publicly available expression matrices for a number of the datasets contained raw counts
646 (retina, hippocampus, hypothalamus, midbrain, visceral motor neurons). For each of these dataset
647 individually, we performed a normalisation step using the *scran* package (version 1.10.2) (Lun et al.,

648 2016) that computes pool-based size factors that are subsequently deconvolved to obtain cell-based
649 size factors.

650 The normalised expression matrices and cell type information were used as input to quantify cell-
651 type specific gene expression. Analysis was performed using the *scde* package (version 1.99.1)
652 (Kharchenko et al., 2014). We modelled the gene expression measurements from each individual cell
653 as a weighted mixture of negative binomial and low-magnitude Poisson distributions. The former
654 accounts for the correlated component in which a transcript is detected and quantified, while the
655 latter accounts for drop-out events in which a transcript fails to amplify when present. The weighting
656 of the two distributions is determined by the level of gene expression in the cell population
657 (Kharchenko et al., 2014). We then used these error models to estimate the likelihood (joint
658 posterior probability) of a gene being expressed at any given average level in a given cell type
659 (Kharchenko et al., 2014). Probability distributions for all nAChR subunit genes detected in all the cell
660 types analysed are shown in sup fig 4. This whole transcriptome analysis provides accurate
661 estimations of gene expression levels, thus allowing for the comparison of individual genes within a
662 given cell type (i.e. the complement of nAChR subunits) or the analysis of expression level
663 differences between cell types (i.e. change in expression level of nAChR subunits between neuronal
664 subtypes). We combined the information about the complement of nAChR subunits for each cell
665 type with a comprehensive catalogue of experimentally validated subunit combinations
666 (Supplementary Table 2 and references therein). We identified the subunit combinations that were
667 present, in each cell type, within a 10-fold, 10 to 100-fold or 100 to 1000 fold range of expression
668 level or absent all together. Admittedly, this analysis approach overlooks the complexities of post-
669 translational modifications, receptor assembly, role of chaperone proteins and transport to the
670 plasma membrane. However, it provides conservative estimates of the maximum potential of
671 combinatorial assembly of subunits and thus a maximum for the repertoire of nAChR assemblies
672 that could be present at the cell membrane.

673 **Expression of recombinant receptors in *Xenopus laevis* oocytes and electrophysiological recordings**

674 Rat and chick α9 and α10 cDNAs subcloned into pSGEM, a modified pGEMHE vector suitable for
675 *Xenopus laevis* oocyte expression studies, were described previously (Elgoyhen et al., 1994; Elgoyhen
676 et al., 2001; Lipovsek et al., 2012). Rat α4, β2 and α7 subunit cDNAs subcloned into pBS SK(−)
677 (Agilent Technologies, Santa Clara, CA) were kindly provided by Dr. Jim Boulter (University of
678 California, Los Angeles, CA). Chicken α4 and β2 subunit cDNAs subcloned into pCI (Promega,
679 Madison, WI) were kindly provided by Dr. Isabel Bermudez-Díaz (Oxford Brookes University, Oxford,
680 UK). Chicken α7 subunit cDNA cloned into pMXT was kindly provided by Dr. Jon Lindstrom
681 (University of Pennsylvania) and was then subcloned into pSGEM between HindIII and SalI sites. Frog

682 α4, β2, α7, α9 and α10 subunits were cloned from whole brain *Xenopus tropicalis* cDNA. Total RNA
683 was prepared from whole brains using the RNAqueous – Micro kit AM1931 (Ambion, Thermo Fisher
684 Scientific, Boston, MA). First strand cDNA synthesis was performed using an oligodT and the
685 ProtoScript Taq RT-PCR kit (New England Biolabs, Ipswich, MA). Second strand synthesis was
686 performed with the NEBNext mRNA Second Strand Synthesis Module kit – E6111S (New England
687 Biolabs, Ipswich, MA). Full length cDNAs for each subunit were PCR amplified (MultiGene 60
688 OptiMaxTM Thermal Cycler - Labnet International Inc. Edison, NJ) using specific primers
689 (Supplementary Table 5). PCR products were sequenced and subcloned into pSGEM between EcoRI
690 and XhoI sites for α9, α7 and β2 nAChRs subunits, between HindIII and XhoI sites for the α10 subunit
691 and between EcoRI and HindIII sites for the α4 subunit. All expression plasmids are readily available
692 upon request.

693 Capped cRNAs were *in vitro* transcribed from linearized plasmid DNA templates using the
694 RiboMAX^{TM} Large Scale RNA Production System-T7 (Promega, Madison, WI). The maintenance of
695 *Xenopus laevis*, as well as the preparation and cRNA injection of stage V and VI oocytes, has been
696 described in detail elsewhere (Katz et al., 2000). Briefly, oocytes were injected with 50 nl of RNase-
697 free water containing 0.01–1.0 ng of cRNAs (at a 1 : 1 molar ratio for α9α10 and α4β2 receptors) and
698 maintained in Barth's solution (in mM): NaCl 88, $Ca(NO_3)_2$ 0.33, $CaCl_2$ 0.41, KCl 1, $MgSO_4$ 0.82,
699 $NaHCO_3$ 2.4, HEPES 10, at 18ºC.

700 Electrophysiological recordings were performed 2 – 6 days after cRNA injection under two-electrode
701 voltage clamp with an Oocyte Clamp OC-725B or C amplifier (Warner Instruments Corp., Hamden,
702 CT). Recordings were filtered at a corner frequency of 10 Hz using a 900BT Tunable Active Filter
703 (Frequency Devices Inc., Ottawa, IL). Data acquisition was performed using a Patch Panel PP-50
704 LAB/1 interface (Warner Instruments Corp., Hamden, CT) at a rate of 10 points per second. Both
705 voltage and current electrodes were filled with 3M KCl and had resistances of ∼1MΩ. Data were
706 analysed using Clampfit from the pClamp 6.1 software (Molecular Devices, Sunnyvale, CA). During
707 electrophysiological recordings, oocytes were continuously superfused (10 ml min^{-1}) with normal
708 frog saline composed of (in mM): 115 NaCl, 2.5 KCl, 1.8 $CaCl_2$ and 10 HEPES buffer, pH 7.2. In order
709 to minimize the activation of the oocyte's native Ca^{2+}-sensitive chloride current (ICl_{Ca}) by inward Ca^{2+}
710 current through the nAChRs, all experiments, unless otherwise stated, were carried out in oocytes
711 incubated with the membrane permeant Ca^{2+} chelator 1,2-bis (2-aminophenoxy)ethane-N,N,N',N'-
712 tetraacetic acid-acetoxymethyl ester (BAPTA-AM; 100 µM) for 3 h prior to electrophysiological
713 recordings. This treatment was previously shown to effectively chelate intracellular Ca^{2+} ions and,
714 therefore, to impair the activation of the ICl_{Ca} (Gerzanich et al., 1994). All recordings were performed
715 at -70 mV holding potential, unless otherwise stated.

716 **Biophysical properties of nAChRs**

717 Concentration-response curves were obtained by measuring responses to increasing concentrations
718 of ACh. Current amplitudes were normalized to the maximal agonist response in each oocyte. The
719 mean and S.E.M. values of the responses are represented. Agonist concentration-response curves
720 were iteratively fitted, using Prism 6 software (GraphPad Software Inc., La Jolla, CA), with the
721 equation: $I/Imax = AnH / (AnH + EC_{50}nH)$, where I is the peak inward current evoked by the agonist at
722 concentration AnH; Imax is current evoked by the concentration of agonist eliciting a maximal
723 response; EC_{50} is the concentration of agonist inducing half-maximal current response and nH is the
724 Hill coefficient.

725 Desensitisation of ACh evoked currents was evaluated via prolonged agonist applications. The
726 percentage of current remaining 5 seconds (for α7 nAChRs) or 20 seconds (for α4β2 and α9α10
727 nAChRs) after the peak of the response was determined for each oocyte.

728 The effects of extracellular Ca^{2+} on the ionic currents through nAChRs were studied by measuring the
729 amplitudes of the responses to a near-EC_{50} concentration of ACh (10 µM for all α4β2 and amniote
730 α9α10 nAChRs, and 100 µM for all α7 and frog α9α10 nAChRs) on extracellular Ca^{2+} ranging from
731 nominally 0 to 3 mM at a holding potential of -90 mV (Weisstaub et al., 2002). These experiments
732 were carried out in oocytes injected with 7.5 ng of an oligonucleotide (5'-
733 GCTTTAGTAATTCCCATCCTGCCATGTTTC-3') antisense to connexinC38 mRNA (Arellano et al., 1995;
734 Ebihara, 1996) to minimise the activation of the oocyte's nonselective inward current through a
735 hemigap junction channel that results from the reduction of external divalent cation concentration.
736 Current amplitudes at each Ca^{2+} concentration were normalized to that obtained in the same oocyte
737 at a 1.8 mM Ca^{2+}.

738 I–V relationships were obtained by applying 2 seconds voltage ramps from -120 to +50 mV from a
739 holding potential of -70 mV, at the plateau response to 3 µM ACh. Leakage correction was
740 performed by digital subtraction of the I–V curve obtained by the same voltage ramp protocol prior
741 to the application of ACh. Generation of voltage protocols and data acquisition were performed
742 using a Patch Panel PP-50 LAB/1 interface (Warner Instruments Corp., Hamden, CT) at a rate of 10
743 points per second and the pClamp 7.0 software (Axon Instruments Corp., Union City, CA). Current
744 values were normalized to the maximum amplitude value obtained for each oocyte. The fast
745 desensitising α7 receptors had negligible plateau currents. For these receptors, responses to 100 µM
746 ACh were obtained at different holding potentials and normalised to the amplitude response at -120
747 mV in the same oocyte.

748 **Statistical analysis**

749 Shapiro-Wilks normality test was conducted using custom routines written in R v3.4.1 (R
750 Development Core Team, 2008), through RStudio software v1.0.153. Statistical significance was
751 determined using either parametric paired *t*-test or One-way ANOVA followed by Holm-Sidak's test,
752 or nonparametric Wilcoxon or Kruskal-Wallis tests followed by Dunn's tests conducted using Prism 6
753 software (GraphPad Software Inc., La Jolla, CA). A $p < 0.05$ was considered significant.

754 **Reagents**

755 All drugs were obtained from Sigma-Aldrich (Buenos Aires, Argentina). ACh chloride was dissolved in
756 distilled water as 100 mM stocks and stored aliquoted at -20°C. BAPTA-AM was stored at -20°C as
757 aliquots of a 100 mM stock solution in dimethylsulfoxide, thawed and diluted into Barth's solution
758 shortly before incubation of the oocytes. ACh solutions in Ringer's saline were freshly prepared
759 immediately before application.

760 **Principal component analysis of functional properties**

761 Principal Component Analysis was performed on the experimental values obtained for the functional
762 properties of extant nAChRs implementing custom routines written in R v3.4.1 and run in RStudio
763 software v1.0.153. Each of the experimental variables was normalized to the maximum value
764 recorded to allow for equal weighting of the properties (Supplementary Table 6). The loadings of the
765 empirical variables on the five principal components (PC) generated are shown in Table 3, alongside
766 the proportion of the total variability explained by each component. The loadings of each biophysical
767 property on each principal component are also shown on the vectors biplot (Figure 8 – inset).

768 **Inference of character state of functional properties of ancestral receptors**

769 The pipeline followed to infer the ancestral character state of biophysical properties of is
770 schematized on Supplementary Figure 5. Briefly, we first reconstructed the ancestral tetrapods and
771 amniote DNA sequences of the α4, α7, α9, α10 and β2 nAChRs subunits (Supplementary File 2). For
772 that purpose, we used the same orthologue sequences that were used to construct the phylogenetic
773 tree of Figure 1, together with a species tree with no branch lengths obtained from Ensembl
774 (https://www.ensembl.org/info/about/speciestree.html). Inferred ancestral DNA sequences for the
775 amniote and tetrapod nodes (Supplementary File 2) were obtained, for all three codon positions, by
776 the maximum likelihood method (Nei and Kumar, 2000) under the Tamura-Nei model (Tamura and
777 Nei, 1993), on the MEGA7 software (Kumar et al., 2016). The initial tree corresponds to the provided
778 Species Tree with very strong restriction to branch swap. The rates among sites were treated as a
779 gamma distribution. All positions with less than 95% site coverage were eliminated.

780 Subsequently, multiple alignments including extant rat, chick and frog and ancestral amniote and
781 tetrapod aminoacid sequences were performed using MEGA7 for each studied nAChR
782 (Supplementary File 3). The sequence identity was used to assign branch length values to α7, α4β2
783 and α9α10 nAChRs trees, corresponding to 1-SeqID (Supplementary Table 7). Theoretical
784 concatemeric constructions were built for the heteromeric α9α10 nAChRs considering the
785 descripted prevalent $(\alpha9)_2(\alpha10)_3$ stoichiometry (Plazas et al., 2005). For the α4β2 nAChRs, the high
786 sensitivity $(\alpha4)_2(\beta2)_3$ stoichiometry was used to generate the theoretical concatemeric receptor
787 (Supplementary File 3). The resulting trees (Supplementary Figure 6) were used, together with the
788 biophysical properties experimentally determined for the extant receptors (Table 2) as input data for
789 ancestral character inference. ACh sensitivity (EC_{50} values), desensitization rates (% of remaining *I* 20
790 sec after ACh peak), Ca^{2+} modulation (*I* elicited by ACh at Ca 0.5 mM/Ca 3 mM), Ca^{2+} permeability (%
791 of remaining *I* after BAPTA treatment) and rectification profile ($I_{+40\ mV}/I_{-90\ mV}$) for the ancestral
792 amniote and tetrapod receptors were inferred using the *ace* function from the *APE* package v5.2
793 (Paradis et al., 2004) implemented in R v3.4.1 and RStudio v1.0.153. We used the Brownian motion
794 model (Schluter et al., 1997) (Schluter et al., 1997), where characters evolve following a random
795 walk fitted by maximum likelihood (Felsenstein, 1973) for the ancestral character estimations of
796 continuous traits. Reconstructed ancestral states are shown in Supplementary Figure 6. Finally, using
797 the loadings of the biophysical properties on PC1 and 2 (Table 3 and Figure 8 – inset), and the
798 normalized experimental (extant receptors) and *in silico* reconstructed (ancestral receptors)
799 biophysical properties results (Supplementary Table 6), we calculated the position of the 15 nAChRs
800 on a bidimensional PCA space (Figure 8).

801

Acknowledgments

This work was supported by Agencia Nacional de Promoción Científicas y Técnicas, Argentina, the Scientific Grand Prize of the Fondation Pour l'Audition and NIH Grant R01 DC001508 (Paul Fuchs PI and ABE co-PI) to ABE.

807 **References**

808 Albuquerque, E.X., Pereira, E.F.R., Alkondon, M., and Rogers, S.W. (2009). Mammalian Nicotinic
809 Acetylcholine Receptors: From Structure to Function. Physiological Reviews 89, 73-120.
810 Arellano, R.O., Woodward, R.M., and Miledi, R. (1995). A monovalent cationic conductance that is
811 blocked by extracellular divalent cations in Xenopus oocytes. J Physiol 484 (Pt 3), 593-604.
812 Arendt, D., Musser, J.M., Baker, C.V.H., Bergman, A., Cepko, C., Erwin, D.H., Pavlicev, M., Schlosser,
813 G., Widder, S., Laubichler, M.D., and Wagner, G.P. (2016). The origin and evolution of cell types.
814 Nature reviews Genetics 17, 744-757.
815 Art, J.J., Fettiplace, R., and Fuchs, P.A. (1984). Synaptic hyperpolarization and inhibition of turtle
816 cochlear hair cells. J Physiol 356, 525-550.
817 Barish, M.E. (1983). A transient calcium-dependent choloride current in the immature Xenopus
818 oocytes. Journal of Physiology 342, 309-325.
819 Bertrand, D., Ballivet, M., and Rungger, D. (2006). Activation and blocking of neuronal nicotinic
820 acetylcholine receptor reconstituted in Xenopus oocytes. Proceedings of the National Academy of
821 Sciences 87, 1993-1997.
822 Bocquet, N., Nury, H., Baaden, M., Le Poupon, C., Changeux, J.P., Delarue, M., and Corringer, P.J.
823 (2009). X-ray structure of a pentameric ligand-gated ion channel in an apparently open
824 conformation. Nature 457, 111-114.
825 Bouzat, C., Nielsen, B.E., and Esandi, C. (2017). Molecular function of α7 nicotinic receptors as drug
826 targets. Journal of Physiology 00, 1-15.
827 Burns, J.C., Kelly, M.C., Hoa, M., Morell, R.J., and Kelley, M.W. (2015). Single-cell RNA-Seq resolves
828 cellular complexity in sensory organs from the neonatal inner ear. Nature Communications 6, 1-16.
829 Castellano-Muñoz, M., Israel, S.H., and Hudspeth, A.J. (2010). Efferent control of the electrical and
830 mechanical properties of hair cells in the bullfrog's sacculus. PLoS ONE 5.
831 Cembrowski, M.S., Phillips, M.G., DiLisio, S.F., Shields, B.C., Winnubst, J., Chandrashekar, J., Bas, E.,
832 and Spruston, N. (2018). Dissociable Structural and Functional Hippocampal Outputs via Distinct
833 Subiculum Cell Classes. Cell 173, 1280--1292.e1218.
834 Chevée, M., Robertson, J.D.J., Cannon, G.H., Brown, S.P., and Goff, L.A. (2018). Variation in Activity
835 State, Axonal Projection, and Position Define the Transcriptional Identity of Individual Neocortical
836 Projection Neurons. Cell Reports 22, 441-455.
837 Corringer, P.J., Poitevin, F., Prevost, M.S., Sauguet, L., Delarue, M., and Changeux, J.P. (2012).
838 Structure and pharmacology of pentameric receptor channels: From bacteria to brain. Structure 20,
839 941-956.
840 Cortese, M., Papal, S., Pisciottano, F., Elgoyhen, A.B., Hardelin, J.-P., Petit, C., Franchini, L.F., and El-
841 Amraoui, A. (2017). Spectrin βV adaptive mutations and changes in subcellular location correlate
842 with emergence of hair cell electromotility in mammalians. Proceedings of the National Academy of
843 Sciences 114, 2054-2059.
844 Couturier, S., Bertrand, D., Matter, J.-M., Hernandez, M.-C., Bertrand, S., Millar, N., Valera, S., Barkas,
845 T., and Ballivet, M. (1990). A neuronal nicotinic acetylcholine receptor subunit (α7) is
846 developmentally regulated and forms a homo-oligomeric channel blocked by α-BTX. Neuron 5, 847-
847 856.
848 Criado, M. (2018). Acetylcholine nicotinic receptor subtypes in chromaffin cells. Pflugers Archiv :
849 European journal of physiology 470, 13-20.
850 Cully, D.F., Vassilatis, D.K., Liu, K.K., Paress, P.S., Van Der Ploeg, L.H.T., Schaeffer, J.M., and Arena, J.P.
851 (1994). Cloning of an avermectin-sensitive glutamate-gated chloride channel from Caenorhabditis
852 elegans. Nature 371, 707-711.
853 Dallos, P. (2008). Cochlear amplification, outer hair cells and prestin. Current opinion in neurobiology
854 18, 370-376.
855 Dani, J.A., and Bertrand, D. (2007). Nicotinic Acetylcholine Receptors and Nicotinic Cholinergic
856 Mechanisms of the Central Nervous System. Annu Rev Pharmacol Toxicol 47, 699-729.

857 Dent, J.A. (2006). Evidence for a diverse Cys-loop ligand-gated ion channel superfamily in early
858 bilateria. Journal of Molecular Evolution 62, 523-535.
859 Ebihara, L. (1996). Xenopus connexin38 forms hemi-gap-junctional channels in the nonjunctional
860 plasma membrane of Xenopus oocytes. Biophysical journal 71, 742-748.
861 Elgoyhen, A.B., Johnson, D.S., Boulter, J., Vetter, D.E., and Heinemann, S. (1994). α9: an acetylcholine
862 receptor with novel pharmacological properties expressed in rat cochlear hair cells. Cell 79, 705-715.
863 Elgoyhen, A.B., and Katz, E. (2012). The efferent medial olivocochlear-hair cell synapse. Journal of
864 Physiology Paris 106, 47-56.
865 Elgoyhen, A.B., Vetter, D.E., Katz, E., Rothlin, C.V., Heinemann, S.F., and Boulter, J. (2001). α10: a
866 Determinant of Nicotinic Cholinergic Receptor Function in Mammalian Vestibular and Cochlear
867 Mechanosensory Hair Cells. Proceedings of the National Academy of Sciences of the United States of
868 America 98, 3501-3506.
869 Felsenstein, J. (1973). Maximum-Likelihood Estimation of Evolutionary Trees from Continuous
870 Characters. Am J Hum Genet 25, 471-492.
871 Felsenstein, J. (1985). Confidence limits on phylogenies: an approach using the bootstrap. Evolution
872 39, 783-791.
873 Franchini, L.F., and Elgoyhen, A.B. (2006). Adaptive evolution in mammalian proteins involved in
874 cochlear outer hair cell electromotility. Molecular Phylogenetics and Evolution 41, 622-635.
875 Fritzsch, B., and Beisel, K.W. (2004). Keeping sensory cells and evolving neurons to connect them to
876 the brain: molecular conservation and novelties in vertebrate ear development. Brain Behav Evol 64,
877 182-197.
878 Fuchs, P.A., and Murrow, B. (1992a). Cholinergic inhibition of short (outer) hair cells of the chick's
879 cochlea. The Journal of neuroscience : the official journal of the Society for Neuroscience 12, 800-
880 809.
881 Fuchs, P.A., and Murrow, B.W. (1992b). A novel cholinergic receptor mediates inhibition of chick
882 cochlear hair cells. Proceedings of the Royal Society of London Series B: Biological Sciences 248, 35-
883 40.
884 Furlan, A., La Manno, G., Lubke, M., Haring, M., Abdo, H., Hochgerner, H., Kupari, J., Usoskin, D.,
885 Airaksinen, M.S., Oliver, G.*, et al.* (2016). Visceral motor neuron diversity delineates a cellular basis
886 for nipple- and pilo-erection muscle control. Nature Neuroscience 19, 1331-1340.
887 Galzi, J.L., Bertrand, S., Corringer, P.J., Changeux, J.P., and Bertrand, D. (1996). Identification of
888 calcium binding sites that regulate potentiation of a neuronal nicotinic acetylcholine receptor. The
889 EMBO journal 15, 5824-5832.
890 Gerzanich, V., Anand, R., and Lindstrom, J.M. (1994). Homomers of α8 and α7 subunits of nicotinic
891 receptors exhibit similar channel but contrasting binding site properties. Molecular Pharmacology
892 45, 212 LP-- 220.
893 Glowatzki, E., and Fuchs, P.A. (2000). Cholinergic synaptic inhibition of inner hair cells in the neonatal
894 mammalian cochlea. Science 288, 2366-2368.
895 Gomez-Casati, M.E., Fuchs, P.A., Elgoyhen, A.B., and Katz, E. (2005). Biophysical and pharmacological
896 characterization of nicotinic cholinergic receptors in rat cochlear inner hair cells. J Physiol 566, 103-
897 118.
898 Goutman, J.D., Fuchs, P.A., and Glowatzki, E. (2005). Facilitating efferent inhibition of inner hair cells
899 in the cochlea of the neonatal rat. Journal of Physiology 566, 49-59.
900 Haghighi, A.P., and Cooper, E. (2000). A molecular link between inward rectification and calcium
901 permeability of neuronal nicotinic acetylcholine α3β4 and α4β2 receptors. The Journal of
902 neuroscience : the official journal of the Society for Neuroscience 20, 529-541.
903 Hao, J., Simard, A.R., Turner, G.H., Wu, J., Whiteaker, P., Lukas, R.J., and Shi, F.D. (2011). Attenuation
904 of CNS inflammatory responses by nicotine involves α7 and non-α7 nicotinic receptors. Experimental
905 Neurology 227, 110-119.
906 Haygood, R., Babbitt, C.C., Fedrigo, O., and Wray, G.A. (2010). Contrasts between adaptive coding
907 and noncoding changes during human evolution. ProcNatlAcadSciUSA 107, 7853-7857.

He, Z., Han, D., Efimova, O., Guijarro, P., Yu, Q., Oleksiak, A., Jiang, S., Anokhin, K., Velichkovsky, B., Grunewald, S., and Khaitovich, P. (2017). Comprehensive transcriptome analysis of neocortical layers in humans, chimpanzees and macaques. Nature Neuroscience 20, 886-895.
Hervé Thany, S. (2010). Insect Nicotinic Acetylcholine Receptors, Vol 683.
Hiel, H., Elgoyhen, A.B., Drescher, D.G., and Morley, B.J. (1996). Expression of nicotinic acetylcholine receptor mRNA in the adult rat peripheral vestibular system. Brain Research 738, 347-352.
Hilf, R.J.C., and Dutzler, R. (2009). Structure of a potentially open state of a proton-activated pentameric ligand-gated ion channel. Nature 457, 115-118.
Hoekstra, H.E., and Coyne, J.A. (2007). The locus of evolution: evo devo and the genetics of adaptation. Evolution 61, 995-1016.
Holt, J.C., Lioudyno, M., Athas, G., Garcia, M.M., Perin, P., and Guth, P.S. (2001). The effect of proteolytic enzymes on the α9-nicotinic receptor-mediated response in isolated frog vestibular hair cells. Hearing Research 152, 25-42.
Hone, A.J., Meyer, E.L., McIntyre, M., and McIntosh, J.M. (2011). Nicotinic acetylcholine receptors in dorsal root ganglion neurons include the α6β4* subtype. The FASEB Journal 26, 917-926.
Hudspeth, A.J. (2008). Making an effort to listen: mechanical amplification in the ear. Neuron 59, 530-545.
Jain, A., Kuryatov, A., Wang, J., Kamenecka, T.M., and Lindstrom, J. (2016). Unorthodox Acetylcholine Binding Sites Formed by alpha5 and beta3 Accessory Subunits in alpha4beta2* Nicotinic Acetylcholine Receptors. The Journal of biological chemistry 291, 23452-23463.
Jaiteh, M., Taly, A., and Hénin, J. (2016). Evolution of pentameric ligand-gated ion channels: Pro-loop receptors. PLoS ONE 11, 1-24.
Jones, D.T., Taylor, W.R., and Thornton, J.M. (1992). The rapid generation of mutation data matrices from protein sequences. Comput Appl Biosci 8, 275-282.
Kalamida, D., Poulas, K., Avramopoulou, V., Fostieri, E., Lagoumintzis, G., Lazaridis, K., Sideri, A., Zouridakis, M., and Tzartos, S.J. (2007). Muscle and neuronal nicotinic acetylcholine receptors: Structure, function and pathogenicity. FEBS Journal 274, 3799-3845.
Karlin, A. (2002). Ion channel structure: Emerging structure of the Nicotinic Acetylcholine receptors. Nature Reviews Neuroscience 3, 102-114.
Katz, E., Verbitsky, M., Rothlin, C.V., Vetter, D.E., Heinemann, S.F., and Elgoyhen, A.B. (2000). High calcium permeability and calcium block of the α9 nicotinic acetylcholine receptor. Hearing research 141, 117-128.
Keiger, C.J.H., Case, L.D., Kendal-Reed, M., Jones, K.R., Drake, A.F., and Walker, J.C. (2003). Nicotinic cholinergic receptor expression in the human nasal mucosa. Ann Otol Rhinol Laryngol 112, 77-84.
Kharchenko, P.V., Silberstein, L., and Scadden, D.T. (2014). Bayesian approach to single-cell differential expression analysis. Nature Methods 11, 740-742.
Koppl, C. (2011). Birds--same thing, but different? Convergent evolution in the avian and mammalian auditory systems provides informative comparative models. Hearing Research 273, 65-71.
Kumar, S., Stecher, G., and Tamura, K. (2016). MEGA7: Molecular Evolutionary Genetics Analysis Version 7.0 for Bigger Datasets. Molecular biology and evolution 33, 1870-1874.
Kuryatov, A., Onksen, J., and Lindstrom, J. (2008). Roles of accessory subunits in alpha4beta2(*) nicotinic receptors. Molecular Pharmacology 74, 132-143.
Kurzen, H., Wessler, I., Kirkpatrick, C.J., Kawashima, K., and Grando, S.A. (2007). The non-neuronal cholinergic system of human skin. Hormone and Metabolic Research 39, 125-135.
La Manno, G., Gyllborg, D., Codeluppi, S., Barker, R.A., Arenas, E., and Linnarsson, S. (2016). Molecular diversity of midbrain development in resource molecular diversity of midbrain development in mouse, human and stem cells. Cell 167, 566-580.
Landisman, C.E., and Connors, B.W. (2007). VPM and PoM nuclei of the rat somatosensory thalamus: Intrinsic neuronal properties and corticothalamic feedback. Cerebral Cortex 17, 2853-2865.

957 Le Novère, N., Corringer, P.-J., and Changeux, J.-P. (2002). The diversity of subunit composition in
958 nAChRs: evolutionary origins, physiologic and pharmacologic consequences. Journal of neurobiology
959 53, 447-456.
960 Lester, H.A., Dibas, M.I., Dahan, D.S., Leite, J.F., and Dougherty, D.A. (2004). Cys-loop receptors: New
961 twists and turns. Trends in Neurosciences 27, 329-336.
962 Liebeskind, B.J., Hillis, D.M., and Zakon, H.H. (2015). Convergence of ion channel genome content in
963 early animal evolution. Proceedings of the National Academy of Sciences 112, E846--E851.
964 Lipovsek, M., Fierro, A., Pérez, E.G., Boffi, J.C., Millar, N.S., Fuchs, P.A., Katz, E., and Elgoyhen, A.B.
965 (2014). Tracking the molecular evolution of calcium permeability in a nicotinic acetylcholine
966 receptor. Molecular Biology and Evolution 31, 3250-3265.
967 Lipovsek, M., Im, G.J., Franchini, L.F., Pisciottano, F., Katz, E., Fuchs, P.A., and Elgoyhen, A.B. (2012).
968 Phylogenetic differences in calcium permeability of the auditory hair cell cholinergic nicotinic
969 receptor. Proceedings of the National Academy of Sciences 109, 4308-4313.
970 Liu, Y., Han, N., Franchini, L.F., Xu, H., Pisciottano, F., Elgoyhen, A.B., Rajan, K.E., and Zhang, S. (2012).
971 The voltage-gated potassium channel subfamily KQT member 4 (KCNQ4) displays parallel evolution
972 in echolocating bats. Molecular Biology and Evolution 29, 1441-1450.
973 Lun, A.T., Bach, K., and Marioni, J.C. (2016). Pooling across cells to normalize single-cell RNA
974 sequencing data with many zero counts. Genome biology 17, 75.
975 Mameli-Engvall, M., Evrard, A., Pons, S., Maskos, U., Svensson, T.H., Changeux, J.P., and Faure, P.
976 (2006). Hierarchical Control of Dopamine Neuron-Firing Patterns by Nicotinic Receptors. Neuron 50,
977 911-921.
978 Manley, G.A. (2017). Comparative Auditory Neuroscience: Understanding the Evolution and Function
979 of Ears. Journal of the Association for Research in Otolaryngology : JARO 18, 1-24.
980 Maskos, U., Molles, B.E., Pons, S., Besson, M., Guiard, B.P., Guilloux, J.P., Evrard, A., Cazala, P.,
981 Cormier, A., Mameli-Engvall, M.*, et al.* (2005). Nicotine reinforcement and cognition restored by
982 targeted expression of nicotinic receptors. Nature 436, 103-107.
983 Mazzaferro, S., Bermudez, I., and Sine, S.M. (2017). α4β2 Nicotinic Acetylcholine Receptors:
984 Relationship between subunit stoichiometry and function at the single channel level. Journal of
985 Biological Chemistry 292, 2729-2740.
986 McCarthy, D.J., Campbell, K.R., Lun, A.T., and Wills, Q.F. (2017). Scater: pre-processing, quality
987 control, normalization and visualization of single-cell RNA-seq data in R. Bioinformatics 33, 1179-
988 1186.
989 McIntosh, J.M., Absalom, N., Chebib, M., Elgoyhen, A.B., and Vincler, M. (2009). Alpha9 nicotinic
990 acetylcholine receptors and the treatment of pain. Biochemical Pharmacology 78, 693-702.
991 McInturff, S., Burns, J.C., and Kelley, M.W. (2018). Characterization of spatial and temporal
992 development of Type I and Type II hair cells in the mouse utricle using new cell-type-specific
993 markers. Biology open 7.
994 Meyer, K.A., Marques-Bonet, T., and Sestan, N. (2017). Differential Gene Expression in the Human
995 Brain Is Associated with Conserved, but Not Accelerated, Noncoding Sequences. Mol Biol Evol 34,
996 1217-1229.
997 Miledi, R., and Parker, I. (1984). Chloride current induced by injection of calcium into Xenopus
998 oocytes. The Journal of Physiology 357, 173-183.
999 Millar, N.S., and Gotti, C. (2009). Diversity of vertebrate nicotinic acetylcholine receptors.
1000 Neuropharmacology 56, 237-246.
1001 Mishina, M., Takai, T., Imoto, K., Noda, M., Takahashi, T., Numa, S., Methfessel, C., and Sakmann, B.
1002 (1986). Molecular distinction between fetal and adult forms of muscle acetylcholine receptor.
1003 Nature 321, 406-411.
1004 Morley, B.J., Li, H.S., Hiel, H., Drescher, D.G., and Elgoyhen, A.B. (1998). Identification of the subunits
1005 of the nicotinic cholinergic receptors in the rat cochlea using RT-PCR and in situ hybridization.
1006 Molecular Brain Research 53, 78-87.

1007 Morley, B.J., Whiteaker, P., and Elgoyhen, A.B. (2018). Commentary: Nicotinic Acetylcholine
1008 Receptor α9 and α10 Subunits Are Expressed in the Brain of Mice. Frontiers in Cellular Neuroscience
1009 12, 10-13.
1010 Moroni, M., Zwart, R., Sher, E., Cassels, B.K., and Bermudez, I. (2006). α4β2 Nicotinic receptors with
1011 high and low acetylcholine sensitivity: Pharmacology, stoichiometry, and sensitivity to long-term
1012 exposure to nicotine. Mol Pharmacol 70, 755-768.
1013 Mulle, C., Léna, C., and Changeux, J.P. (1992). Potentiation of nicotinic receptor response by external
1014 calcium in rat central neurons. Neuron 8, 937-945.
1015 Nei, M., and Kumar, S. (2000). Molecular Evolution and Phylogenetics (New York: Oxford Press).
1016 Nielsen, R., Bustamante, C., Clark, A.G., Glanowski, S., Sackton, T.B., Hubisz, M.J., Fledel-Alon, A.,
1017 Tanenbaum, D.M., Civello, D., White, T.J.*, et al.* (2005). A scan for positively selected genes in the
1018 genomes of humans and chimpanzees. PLoS biology 3, e170.
1019 Oliver, D., He, D.Z.Z., Klöcker, N., Ludwig, J., Schulte, U., Siegfried, W., Ruppersberg, J.P., Dallos, P.,
1020 and Fakle, B. (2001). Intracellular Anions as the Voltage Sensor of Prestin , the Outer Hair Cell Motor
1021 Protein. Science 292, 2340-2344.
1022 Ortells, M., and Lunt, G.G. (1995). History of the Ligand-Gated Superfamily of Receptors. Trends
1023 neuroscience 18, 121-127.
1024 Pan, J., Chen, Q., Willenbring, D., Yoshida, K., Tillman, T., Kashlan, O.B., Cohen, A., Kong, X.P., Xu, Y.,
1025 and Tang, P. (2012). Structure of the pentameric ligand-gated ion channel ELIC cocrystallized with its
1026 competitive antagonist acetylcholine. Nature Communications 3, 714-718.
1027 Papke, R.L., and Porter Papke, J.K. (2002). Comparative pharmacology of rat and human α7 nAChR
1028 conducted with net charge analysis. British Journal of Pharmacology 137, 49-61.
1029 Paradis, E., Claude, J., and Strimmer, K. (2004). APE: Analyses of phylogenetics and evolution in R
1030 language. Bioinformatics 20, 289-290.
1031 Parks, X.X., Contini, D., Jordan, P.M., and Holt, J.C. (2017). Confirming a Role for α9 nAChRs and SK
1032 Potassium Channels in Type II Hair Cells of the Turtle Posterior. Frontiers in Cellular Neuroscience 11,
1033 1-18.
1034 Pedersen, J.E., Bergqvist, C.A., and Larhammar, D. (2019). Evolution of vertebrate nicotinic
1035 acetylcholine receptors. BMC Evolutionary Biology 19, 1-21.
1036 Petitpre, C., Wu, H., Sharma, A., Tokarska, A., Fontanet, P., Wang, Y., Helmbacher, F., Yackle, K.,
1037 Silberberg, G., Hadjab, S., and Lallemend, F. (2018). Neuronal heterogeneity and stereotyped
1038 connectivity in the auditory afferent system. Nature Communications 9, 3691.
1039 Picciotto, M.R., and Corrigall, W.A. (2002). Neuronal systems underlying behaviors related to
1040 nicotine addiction: neural circuits and molecular genetics. The Journal of neuroscience : the official
1041 journal of the Society for Neuroscience 22, 3338-3341.
1042 Picciotto, M.R., Zoli, M., Rimondini, R., Léna, C., Marubio, L.M., Pich, E.M., Fuxe, K., and Changeux,
1043 J.P. (1998). Acetylcholine receptors containing the β2 subunit are involved in the reinforcing
1044 properties of nicotine. Nature 391, 173-177.
1045 Pisciottano, F., Cinalli, A.R., Stopiello, M., and Castagna, V.C. (2019). Positive Selection and
1046 Adaptation of Novel Inner Ear Genes in the Mammalian Lineage. Molecular Biology and Evolution.
1047 Proulx, E., Piva, M., Tian, M.K., Bailey, C.D.C., and Lambe, E.K. (2014). Nicotinic acetylcholine
1048 receptors in attention circuitry: The role of layer VI neurons of prefrontal cortex. Cellular and
1049 Molecular Life Sciences 71, 1225-1244.
1050 Quick, M.W., and Lester, R.A.J. (2002). Desensitization of neuronal nicotinic receptors. Journal of
1051 Neurobiology 53, 457-478.
1052 Ramirez-Latorre, J., Yu, C.R., Qu, X., Perin, F., Karlin, A., and Role, L. (1996). Functional contributions
1053 of α5 subunit to neuronal acetylcholine receptor channels. Nature 380, 347-351.
1054 Rau, K.K., Johnson, R.D., and Cooper, B.Y. (2004). Nicotinic AChR in Subclassified Capsaicin-Sensitive
1055 and -Insensitive Nociceptors of the Rat DRG. Journal of Neurophysiology 93, 1358-1371.
1056 Reijntjes, D.O.J., and Pyott, S.J. (2016). The afferent signaling complex: Regulation of type I spiral
1057 ganglion neuron responses in the auditory periphery. Hear Res 336, 1-16.

Romanov, R.A., Zeisel, A., Bakker, J., Girach, F., Hellysaz, A., Tomer, R., Alpár, A., Mulder, J., Clotman, F., Keimpema, E.*, et al.* (2017). Molecular interrogation of hypothalamic organization reveals distinct dopamine neuronal subtypes. Nature Neuroscience 20, 176-188.

Roux, I., Wu, J.S., McIntosh, J.M., and Glowatzki, E. (2016). Assessment of the expression and role of the α1 -nAChR subunit in efferent cholinergic function during the development of the mammalian cochlea. Journal of Neurophysiology 116, 479-492.

Roux, J., Liu, J., and Robinson-Rechavi, M. (2017). Selective constraints on coding sequences of nervous system genes are a major determinant of duplicate gene retention in vertebrates. Molecular Biology and Evolution 34, 2773-2791.

Rzhetsky, A., and Nei, M. (1992). A simple method for estimating and testing minimum-evolution trees. Mol Biol Evol 9, 945-967.

Saitou, N., and Nei, M. (1987). The neighbor-joining method: A new method for reconstructing phylogenetic trees. Mol Biol Evol 4, 406-425.

Samaranayake, H., Saunders, J.C., Greene, M.I., and Navaratnam, D.S. (2004). Ca2+ and K+ (BK) channels in chick hair cells are clustered and colocalized with apical-basal and tonotopic gradients. Journal of Physiology 560, 13-20.

Sands, S.B., and Barish, M.E. (1992). Neuronal nicotinic acetylcholine receptor currents in phaeochromocytoma (pc12) cells: dual mechanisms of rectification. Journal of Physiology, 467-487.

Sato, K.Z., Fujii, T., Watanabe, Y., Yamada, S., Ando, T., Kazuko, F., and Kawashima, K. (1999). Diversity of mRNA expression for muscarinic acetylcholine receptor subtypes and neuronal nicotinic acetylcholine receptor subunits in human mononuclear leukocytes and leukemic cell lines. Neuroscience Letters 266, 17-20.

Scheffer, D., Sage, C., Plazas, P.V., Huang, M., Wedemeyer, C., Zhang, D.-S., Chen, Z.-Y., Elgoyhen, A.B., Corey, D.P., and Pingault, V. (2007). The α1 subunit of nicotinic acetylcholine receptors in the inner ear: transcriptional regulation by ATOH1 and co-expression with the γ subunit in hair cells. Journal of Neurochemistry 0, 071027034430002--???

Schluter, D., Price, T., Mooers, A., and Ludwig, D. (1997). Likelihood of Ancestors States in Adaptive Radiation. Evolution 51, 1699-1711.

Schultz, W. (2007). Multiple Dopamine Functions at Different Time Courses. Annual Review of Neuroscience 30, 259-288.

Séguéla, P., Wadiche, J., Dineley-Miller, K., Dani, J.A., and Patrick, J.W. (1993). Molecular cloning, functional properties, and distribution of rat brain alpha 7: a nicotinic cation channel highly permeable to calcium. The Journal of neuroscience : the official journal of the Society for Neuroscience 13, 596-604.

Sgard, F., Charpantier, E., Bertrand, S., Walker, N., Caput, D., Graham, D., Bertrand, D., and Besnard, F. (2002). A novel human nicotinic receptor subunit, alpha10, that confers functionality to the alpha9-subunit. Molecular Pharmacology 61, 150-159.

Shekhar, K., Lapan, S.W., Whitney, I.E., Tran, N.M., Macosko, E.Z., Kowalczyk, M., Adiconis, X., Levin, J.Z., Nemesh, J., Goldman, M.*, et al.* (2016). Comprehensive Classification of Retinal Bipolar Neurons by Single-Cell Transcriptomics. Cell 166, 1308--1323.e1330.

Shrestha, B.R., Chia, C., Wu, L., Kujawa, S.G., Liberman, M.C., Goodrich, L.V., Shrestha, B.R., Chia, C., Wu, L., Kujawa, S.G.*, et al.* (2018). Sensory neuron diversity in the inner ear is shaped by activity sensory neuron diversity. Cell 174, 1229-1246.

Sienknecht, U.J., Köppl, C., and Fritzsch, B. (2014). Evolution and development of hair cell polarity and efferent function in the inner ear. Brain, Behavior and Evolution 83, 150-161.

Spurny, R., Ramerstorfer, J., Price, K., Brams, M., Ernst, M., Nury, H., Verheij, M., Legrand, P., Bertrand, D., Bertrand, S.*, et al.* (2012). Pentameric ligand-gated ion channel ELIC is activated by GABA and modulated by benzodiazepines. ProcNatlAcadSciUSA 109, 3028-3034.

Steinbach, J.H. (1989). Structural and functional diversity in vertebrate skeletal muscle nicotinic acetylcholine receptors. Ann Rev Physiol, 353-365.

1108 Sugino, K., Clark, E., Schulmann, A., Shima, Y., Wang, L., Hunt, D.L., Hooks, B.M., Traenkner, D.,
1109 Chandrashekar, J., Picard, S.*, et al.* (2019). Mapping the transcriptional diversity of genetically and
1110 anatomically defined cell populations in the mouse brain. eLife 8.
1111 Sun, S., Babola, T., Pregernig, G., So, K.S., Nguyen, M., Su, S.M., Palermo, A.T., Bergles, D.E., Burns,
1112 J.C., and Muller, U. (2018). Hair Cell Mechanotransduction Regulates Spontaneous Activity and Spiral
1113 Ganglion Subtype Specification in the Auditory System. Cell 174, 1247-1263 e1215.
1114 Tamura, K., and Nei, M. (1993). Estimation of the number of nucleotide substitutions in the control
1115 region of mitochondrial DNA in humans and chimpanzees. Mol Biol Evol 10, 512-526.
1116 Tapia, L., Kuryatov, A., and Lindstrom, J. (2007). Ca2+ Permeability of the (α4)3(β2)2 Stoichiometry
1117 Greatly Exceeds That of (α4)2(β2)3 Human Acetylcholine Receptors. Molecular Pharmacology 71,
1118 769-776.
1119 Tasneem, A., Iyer, L.M., Jakobsson, E., and Aravind, L. (2005). Identification of the prokaryotic ligand-
1120 gated ion channels and their implications for the mechanisms and origins of animal Cys-loop ion
1121 channels. Genome biology 6, R4-R4.
1122 Tian, M.K., Bailey, C.D., and Lambe, E.K. (2014). Cholinergic excitation in mouse primary vs.
1123 associative cortex: region-specific magnitude and receptor balance. The European journal of
1124 neuroscience 40, 2608-2618.
1125 Traynelis, S.F., Wollmuth, L.P., McBain, C.J., Menniti, F.S., Vance, K.M., Ogden, K.K., Hansen, K.B.,
1126 Yuan, H., Myers, S.J., and Dingledine, R. (2010). Glutamate receptor ion channels: Structure,
1127 regulation, and function. Pharmacological Reviews 62, 405-496.
1128 Tsang, S.Y., Ng, S.K., Xu, Z., and Xue, H. (2007). The evolution of GABAA receptor-like genes.
1129 Molecular Biology and Evolution 24, 599-610.
1130 Tsunoyama, K., and Gojobori, T. (1998). Evolution of Nicotinic Acetylcholine Receptor Subunits. Mol
1131 Biol Evol 15, 518-527.
1132 Tucker, A.S. (2017). Major evolutionary transitions and innovations: the tympanic middle ear.
1133 Philosophical transactions of the Royal Society of London Series B, Biological sciences 372.
1134 Usoskin, D., Furlan, A., Islam, S., Abdo, H., Lönnerberg, P., Lou, D., Hjerling-Leffler, J., Haeggström, J.,
1135 Kharchenko, O., Kharchenko, P.V.*, et al.* (2015). Unbiased classification of sensory neuron types by
1136 large-scale single-cell RNA sequencing. Nature Neuroscience 18, 145-153.
1137 Vernino, S., Amador, M., Luetje, C.W., Patrick, J., and Dani, J.A. (1992). Calcium modulation and high
1138 calcium permeability of neuronal nicotinic acetylcholine receptors. Neuron 8, 127-134.
1139 Vetter, D.E., Katz, E., Maison, S.F., Taranda, J., Turcan, S., Ballestero, J., Liberman, M.C., Elgoyhen,
1140 A.B., and Boulter, J. (2007). The a10 nicotinic acetylcholine receptor subunit is required for normal
1141 synaptic function and integrity of the olivocochlear system. ProcNatlAcadSciUSA 104, 20594-20599.
1142 Waelti, P., Dickinson, A., and Schultz, W. (2001). Dopamine responses comply with basic
1143 assumptions of formal learning theory. Nature 412, 43-48.
1144 Weisstaub, N., Vetter, D.E., Elgoyhen, A.B., and Katz, E. (2002). The α9α10 nicotinic acetylcholine
1145 receptor is permeable to and is modulated by divalent cations. Hearing research 167, 122-135.
1146 Wersinger, E., McLean, W.J., Fuchs, P.A., and Pyott, S.J. (2010). BK Channels Mediate Cholinergic
1147 Inhibition of High Frequency Cochlear Hair Cells. PLoS ONE 5, e13836-e13836.
1148 Zakrzewicz, A., Richter, K., Agne, A., Wilker, S., Siebers, K., Fink, B., Krasteva-Christ, G., Althaus, M.,
1149 Padberg, W., Hone, A.J.*, et al.* (2017). Canonical and Novel Non-Canonical Cholinergic Agonists
1150 Inhibit ATP-Induced Release of Monocytic Interleukin-1beta via Different Combinations of Nicotinic
1151 Acetylcholine Receptor Subunits alpha7, alpha9 and alpha10. Frontiers in Cellular Neuroscience 11,
1152 189.
1153 Zarghooni, S., Wunsch, J., Bodenbenner, M., Brüggmann, D., Grando, S.A., Schwantes, U., Wess, J.,
1154 Kummer, W., and Lips, K.S. (2007). Expression of muscarinic and nicotinic acetylcholine receptors in
1155 the mouse urothelium. Life Sciences 80, 2308-2313.
1156 Zheng, Y., Hirschberg, B., Yuan, J., Wang, A.P., Hunt, D.C., Ludmerer, S.W., Schmatz, D.M., and Cully,
1157 D.F. (2002). Identification of two novel Drosophila melanogaster histamine-gated chloride channel
1158 subunits expressed in the eye. Journal of Biological Chemistry 277, 2000-2005.

1159 Zoli, M., Pistillo, F., and Gotti, C. (2015). Diversity of native nicotinic receptor subtypes in mammalian
1160 brain. Neuropharmacology 96, 302-311.
1161 Zoli, M., Pucci, S., Vilella, A., and Gotti, C. (2018). Neuronal and Extraneuronal Nicotinic Acetylcholine
1162 Receptors. Current neuropharmacology 16, 338-349.
1163 Zwart, R., and Vijverberg, H.P.M. (1998). Four Pharmacologically Distinct Subtypes of a4b2 Nicotinic
1164 Acetylcholine Receptor Expressed in Xenopus laevis Oocytes. Molecular pharmacology 54, 1124-
1165 1131.

1166

1167

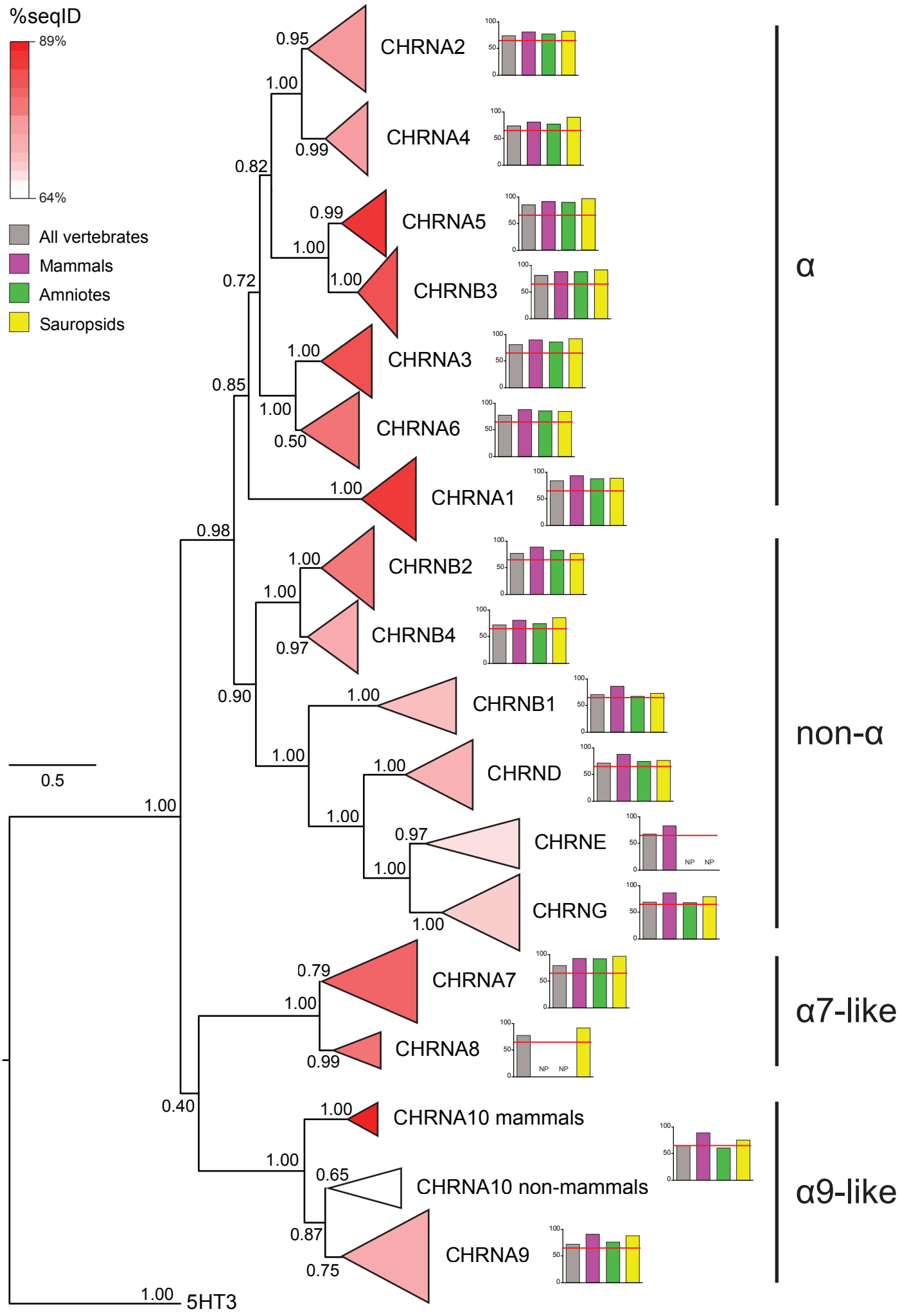
%seqID
89%
64%
All vertebrates
Mammals
Amniotes
Sauropsids
0.5
CHRNA2
CHRNA4
CHRNA5
CHRNB3
CHRNA3
CHRNA6
CHRNA1
CHRNB2
CHRNB4
CHRNB1
CHRND
CHRNE
CHRNG
CHRNA7
CHRNA8
CHRNA10 mammals
CHRNA10 non-mammals
CHRNA9
5HT3
α
non-α
α7-like
α9-like
NP
NP

Figure 1. Hair cell nAChR subunits show greater sequence divergence than neuronal subunits. Phylogenetic relationships between vertebrate nicotinic subunits as obtained from a minimum evolution tree with variation rate among sites modelled by a gamma distribution. The branches corresponding to the same subunits of different species were collapsed up to the node at which one subunit separates from its closest neighbour. The complete tree is shown in supplementary Figure 1. Triangles height indicates the number of individual sequences within each collapsed branch. Triangles length denotes the divergence on sequence identity from the subunit node. Triangles were coloured according to the average percentage of sequence identity between all pairs of sequences (%seqID, Table 1) within the branch. Numbers in branches indicate the bootstrap value obtained after 1,000 replicates. Scale bar indicates the number of amino acid substitutions per site. Histograms next to each subunit branch indicate the average %seqID for all vertebrates (grey), mammals (pink), mammals vs sauropsids (i.e. amniotes) (green) and sauropsids (yellow). The horizontal red line corresponds to the %seqID of the α10 subunit sequences from all vertebrates. NP = not present.

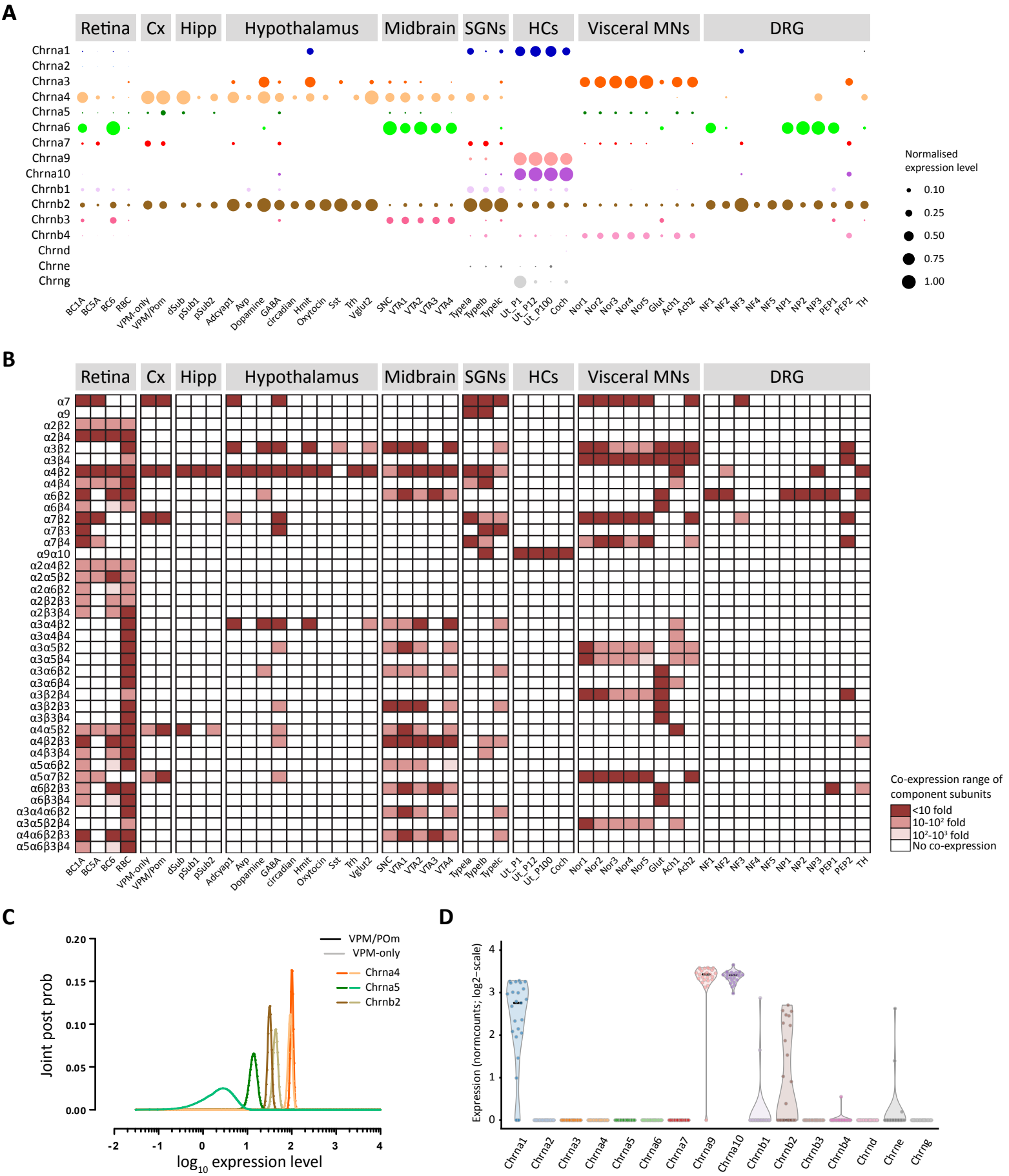

Figure 2. Hair cell nAChR subunits are co-expressed in inner ear hair cells, while neuronal subunits show widespread and variable co-expression patterns. A. Normalised mean expression level for nAChR subunits across mouse neuronal and sensory cell types. Circle sizes indicate the mean expression level for each cell type, normalised to the highest value observed within each dataset. For detailed explanations of individual cell types refer to main text, methods section or the original publications. **B.** Co-expression of subunits comprising known nAChR assemblies. Dark red squares, all component subunits are co-expressed within a 10-fold range of expression level. Light red squares, all component subunits are co-expressed within a 100-fold range of expression level. Pink squares, all component subunits are expressed within a 1000-fold range of expression level. White squares, at least one subunit of that receptor assembly in not expressed in that cell type. **C.** Estimated joint posterior probability distributions for expression levels of Chrna4, Chrna5 and Chrnb2 in VPM-only and VPM/POm projecting layer VI neurons. **D.** Violin plots of expression level of all nAChR subunits in adult utricle hair cells.

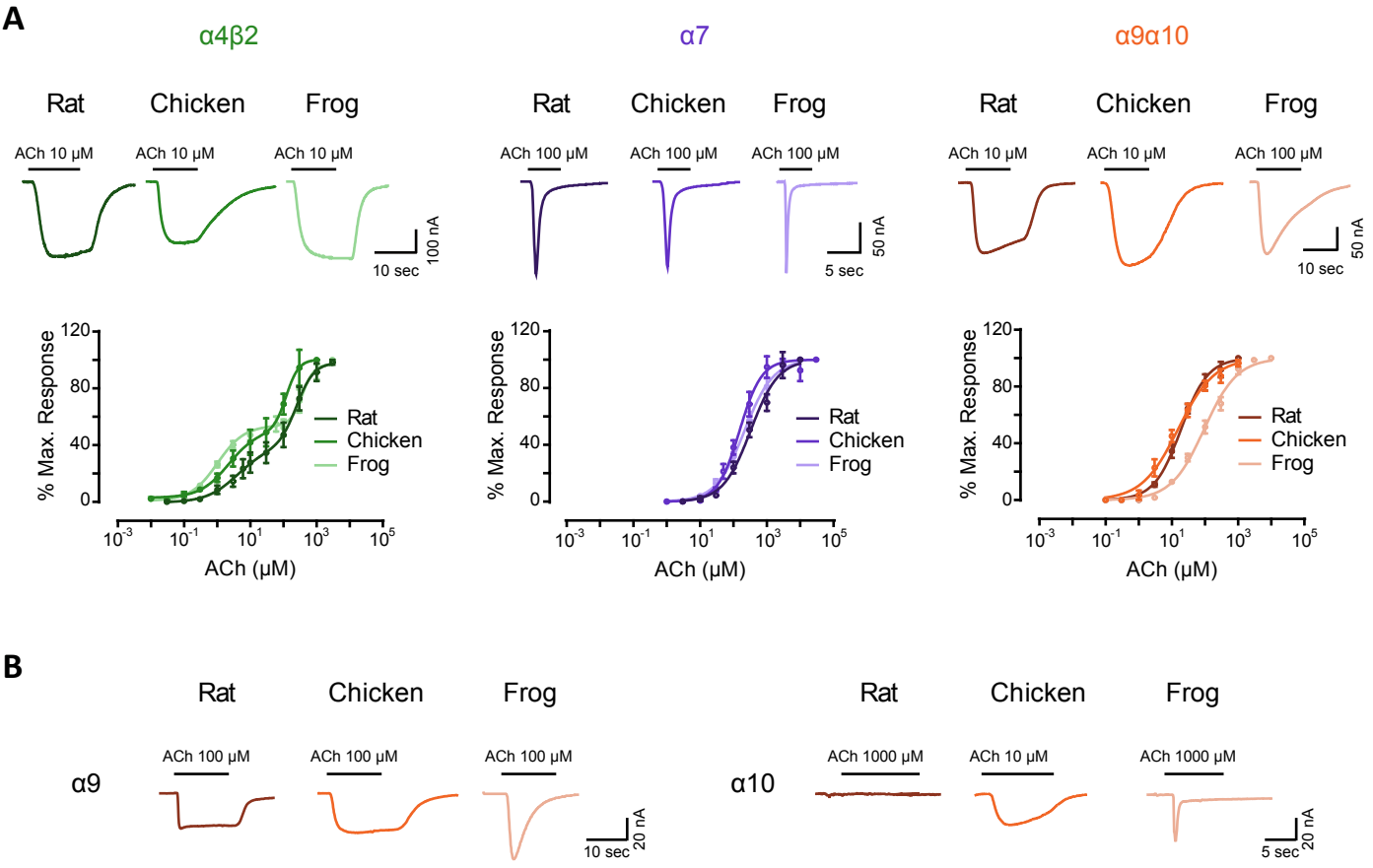

Figure 3. Hair cell nAChRs show differences in ACh apparent affinity, while neuronal nAChRs have similar ACh sensitivity. A. *Top panels.* Representative responses evoked by ACh in oocytes expressing rat, chicken or frog α4+β2, α7 or α9+α10 nAChRs subunits. *Bottom panels.* Concentration-response curves for neuronal α4β2 and α7 nAChRs and hair cell α9α10 nAChRs from the three tetrapod species. Values are mean ± S.E.M. Lines are best fit to the Hill equation (n = 4-9). **B.** Representative responses evoked by ACh in oocytes injected with either rat, chicken or frog homomeric α9 and α10 subunits (n=2–20).

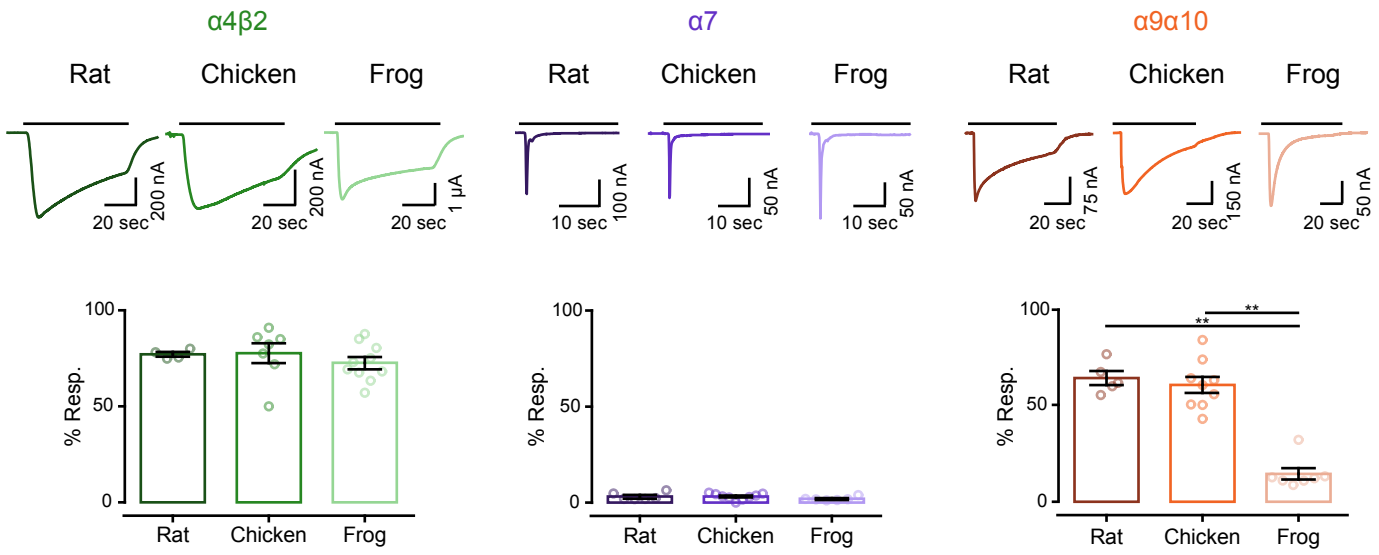

Figure 4. Hair cell nAChRs differ in their desensitization patterns, while neuronal receptors show similar profiles. *Top panels.* Representative responses of α4β2, α7 and α9α10 nAChRs to a 60 seconds (for α4β2 and α9α10) or 30 seconds (for α7) application of 100 μM ACh for all α4β2 and amniotes α9α10, and 1 mM ACh for all α7 and frog α9α10 nAChRs. *Bottom panels.* Percentage of current remaining 20 seconds (α9α10 and α4β2) or 5 seconds (α7) after the peak response, relative to the maximum current amplitude elicited by ACh. Bars represent mean ± S.E.M., open circles represent individual oocytes (n = 4-10). **p<0.01, One-Way ANOVA followed by Dunn's test (α4β2 nAChRs) or Kruskal-Wallis followed by Holm Sidak's test (α7 and α9α10 nAChRs).

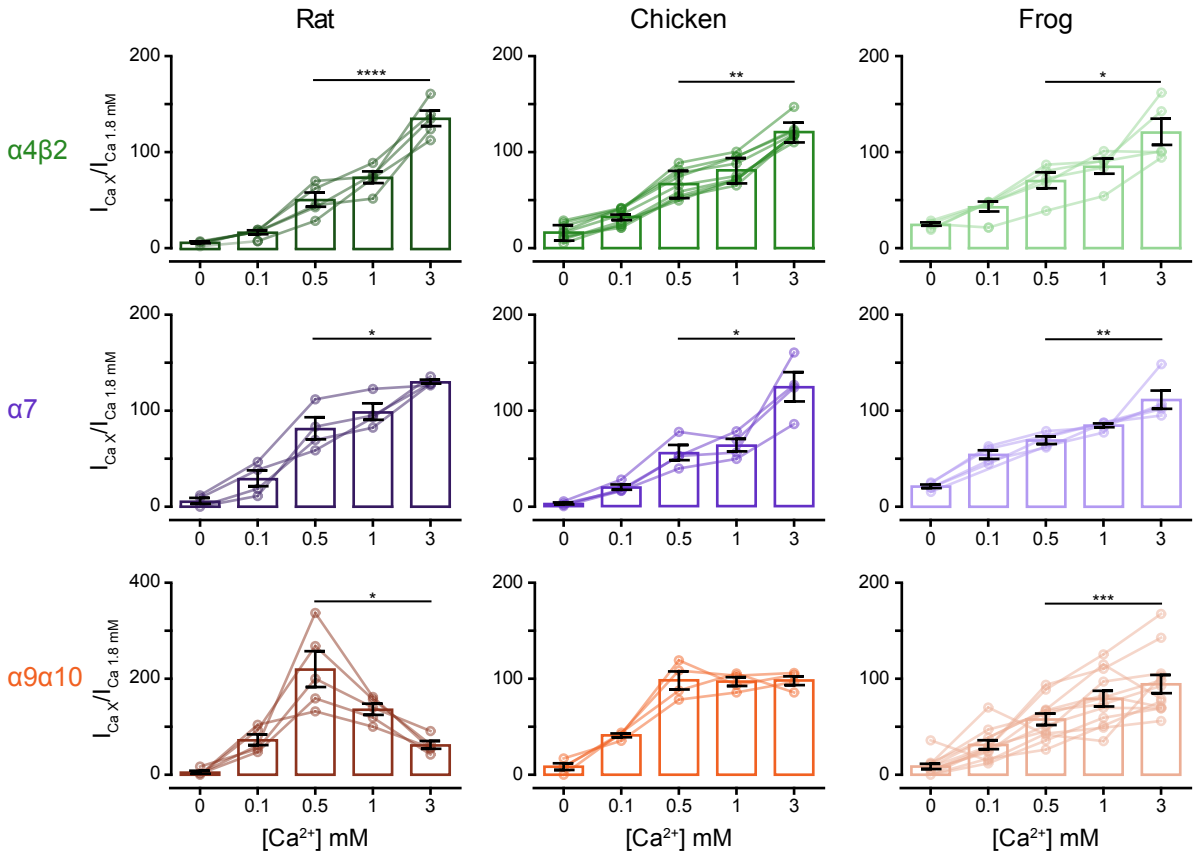

Figure 5. Extracellular Ca2+ potentiates neuronal nAChRs but differentially modulates α9α10 nAChRs. ACh response amplitude as a function of extracellular Ca2+ concentration. ACh was applied at near-EC50 concentrations (10 µM ACh for all α4β2, rat and chick α9α10 nAChRs and 100 µM ACh for all α7 and frog α9α10 nAChRs). Current amplitudes recorded at different Ca2+ concentrations in each oocyte were normalized to the response obtained at 1.8 mM Ca2+ in the same oocyte. Holding voltage: -90 mV. Bars represent mean ± S.E.M., open circles represent individual oocytes (n = 4-12). *p<0.05, **p<0.01, ***p<0.005, ****p<0.0001, Paired t-test (rat and frog α4β2 nAChRs and all α7 and α9α10 nAChRs) or Wilcoxon matched pair test (chick α4β2 nAChR) – comparing 0.5 mM Ca2+ vs 3 mM Ca2+.

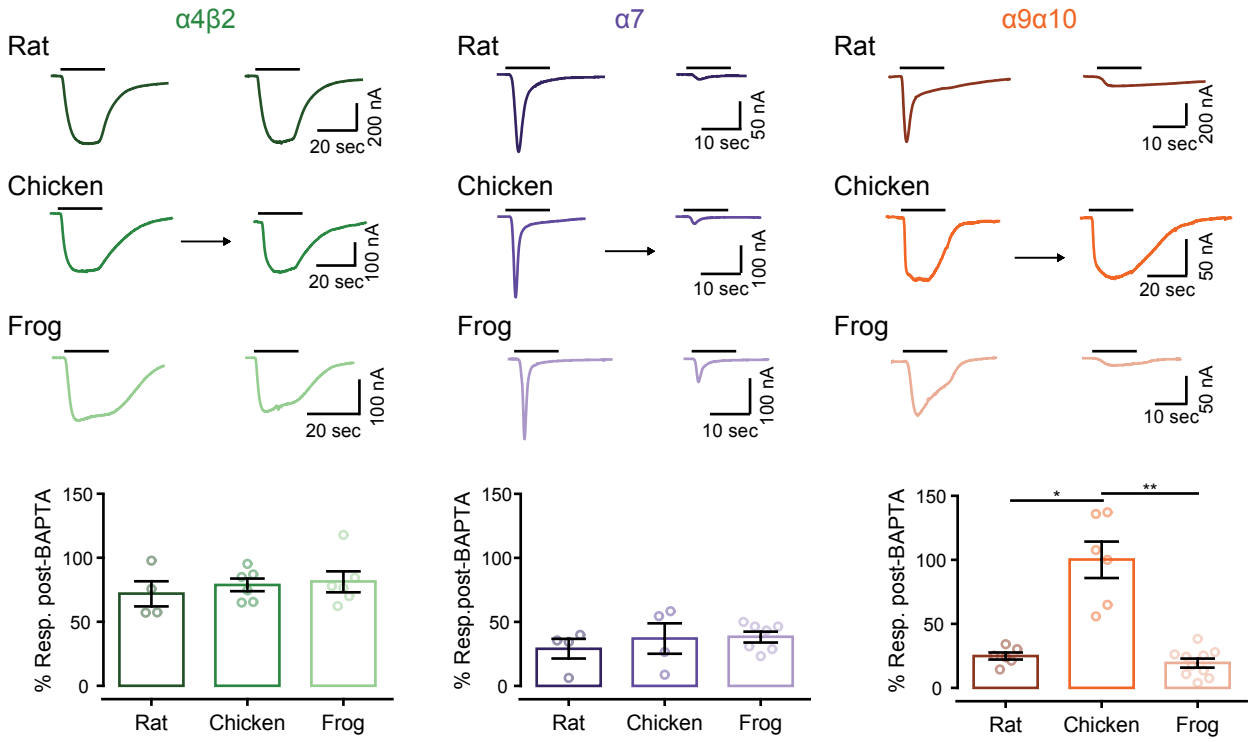

Figure 6. Unlike neuronal nAChRs, α9α10 nAChRs exhibit differential Ca2+ contribution to the total inward current. *Top panels.* Representative responses to near-EC50 concentration of ACh (10 µM ACh for all α4β2 and amniotes α9α10 nAChRs and 100 µM ACh for all α7 and frog α9α10 nAChRs) in oocytes expressing α4β2, α7 and α9α10 nAChRs, before and after a 3 hour incubation with BAPTA-AM (Vh= −70 mV). *Bottom panels.* Percentage of the initial response remaining after BAPTA incubation. Bars represent mean ± S.E.M., open circles represent individual oocytes (n = 4-10). ****p<0.0001, One-Way ANOVA followed by Dunn's test (α4β2 and α7 nAChRs) or Kruskal-Wallis followed by Holm Sidak's test (α9α10 nAChRs).

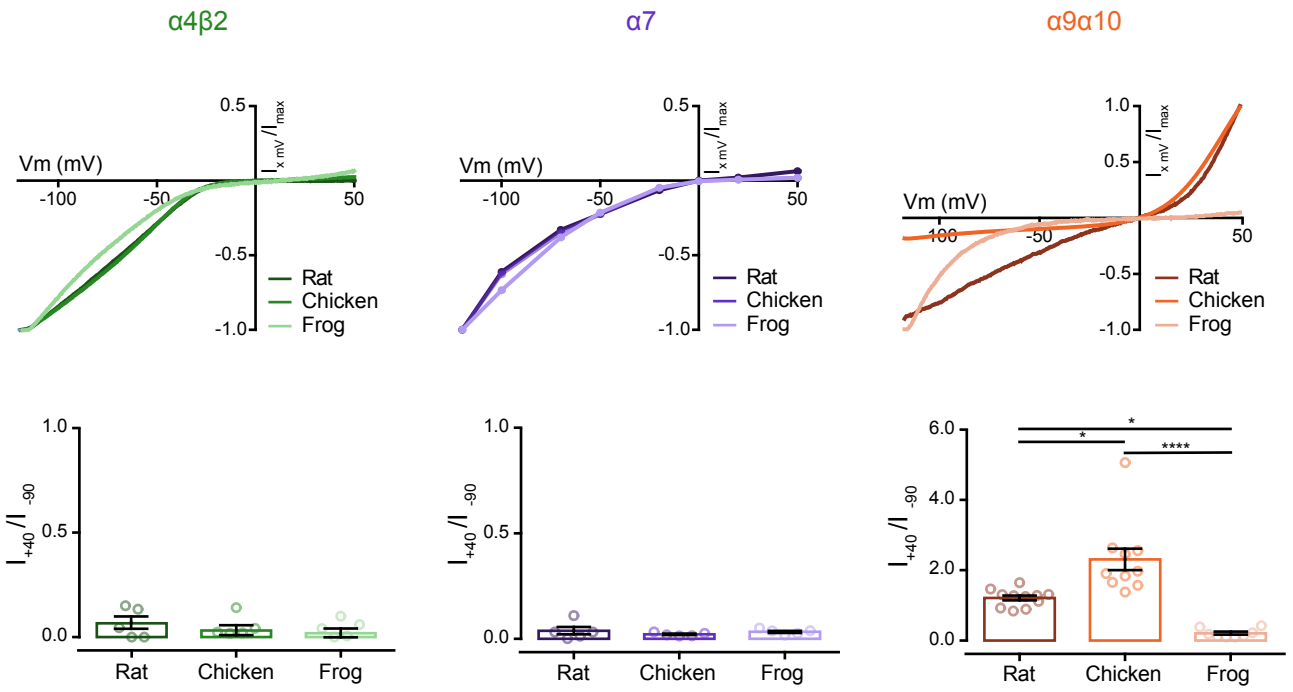

Figure 7. Hair cell, but not neuronal, nAChRs show differential current-voltage relationships across species. *Top panels.* Representative I–V curves obtained by the application of voltage ramps (-120 to +50mV, 2 seconds) at the plateau response to 3 µM ACh for α4β2 and α9α10 or by the application of 100 µM ACh at different holding potentials for α7 nAChRs. Values were normalized to the maximal agonist response obtained for each receptor. *Bottom panels.* Ratio of current amplitude at +40 mV relative to -90 mV for each oocyte. Bars represent mean ± S.E.M., open circles represent individual oocytes (n = 5-11). *p<0.05 ****p< 0.0001, One-Way ANOVA followed by Dunn's test (α4β2 and α7 nAChRs) or Kruskal-Wallis followed by Holm Sidak's test (α9α10 nAChRs).

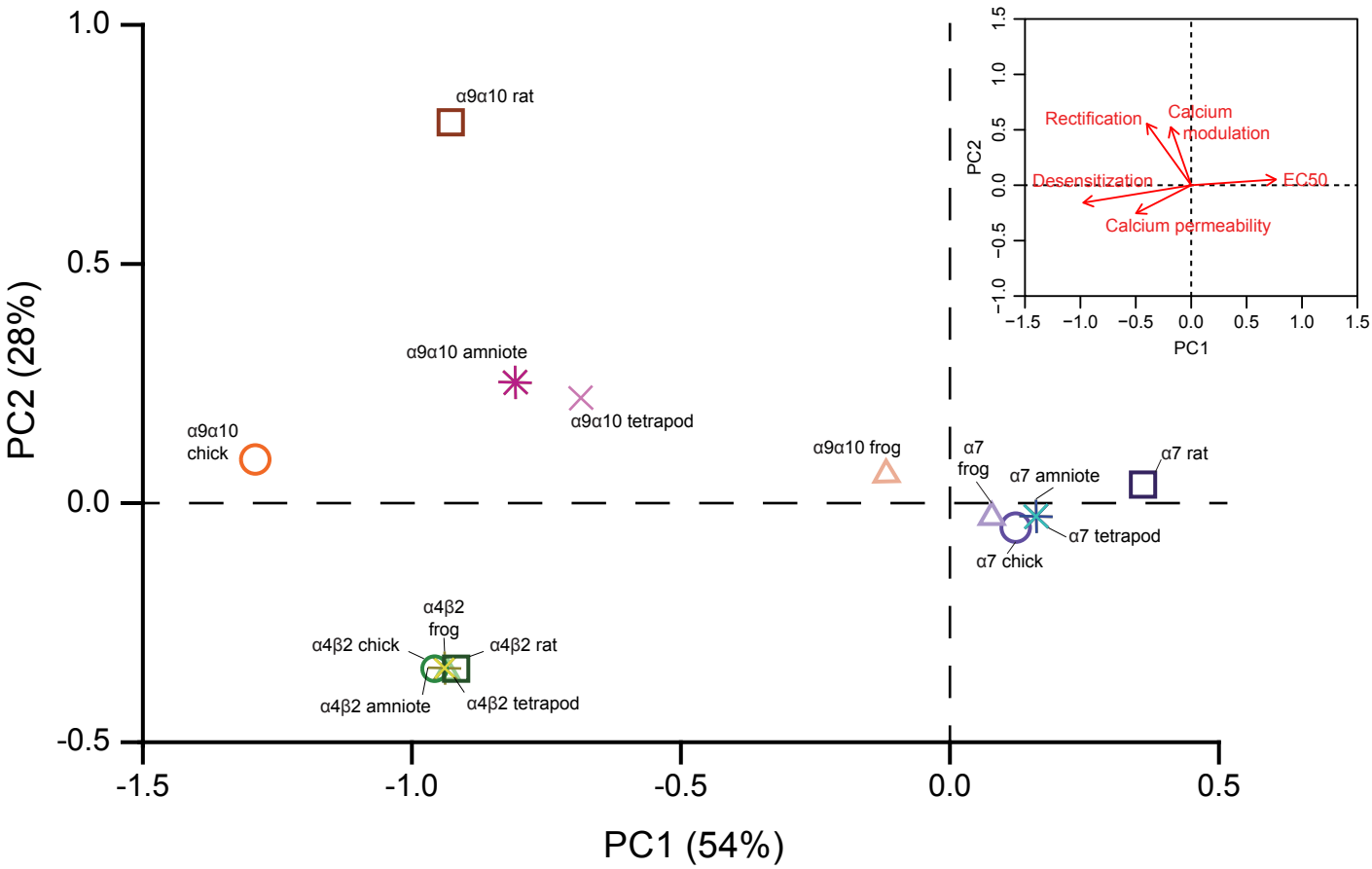

Figure 8. Hair cell nAChRs show great functional divergence, while functional properties of neuronal nAChRs are conserved. PCA was conducted using the experimentally determined biophysical properties (Supplementary Table 6). Square symbols represent rat nAChRs, circles represent chick nAChRs and triangles represent frog nAChRs, α4β2 nAChRs are shown in shades of green, α7 nAChRs in shades of purple and α9α10 nAChRs in shades of orange. The projected placement of inferred functional states for amniote (stars) and tetrapod (crosses) ancestral receptors are coloured in grades of yellow (α4β2), blue (α7) or pink (α9α10). Inset. Biplot of the relative contribution of the five biophysical properties to PC1 and PC2.

	All	Mammals	Mammals-Sauropsid	Sauropsid
CHRNA1	83.98 (26)	93.40 (11)	85.44	88.98 (9)
CHRNA2	73.99 (24)	81.02 (11)	71.68	82.21 (7)
CHRNA3	80.91 (23)	89.78 (10)	83.50	91.79 (8)
CHRNA4	73.63 (26)	80.77 (11)	74.14	90.06 (9)
CHRNA5	84.55 (21)	90.65 (9)	86.18	96.27 (7)
CHRNA6	77.61 (24)	88.09 (11)	80.31	84.93 (8)
CHRNA7	79.22 (26)	92.97 (9)	89.69	96.97 (8)
CHRNA8	77.63 (12)	-	-	91.49 (6)
CHRNA9	72.16 (29)	90.90 (11)	74.23	88.28 (9)
CHRNA10	64.93 (24)	88.98 (11)	61.29	75.38 (5)
CHRNB1	70.47 (18)	86.24 (11)	63.82	73.20 (3)
CHRNB2	77.16 (26)	88.70 (11)	75.83	76.87 (9)
CHRNB3	81.47 (28)	88.41 (11)	84.59	91.83 (8)
CHRNB4	72.12 (23)	80.83 (10)	71.75	85.65 (7)
CHRND	71.54 (22)	87.85 (10)	68.02	76.59 (6)
CHRNE	67.34 (16)	83.08 (10)	58.60	-
CHRNG	69.12 (24)	86.81 (11)	63.41	79.55 (8)

Table 1. Mean percentage sequence identity (%seqID). Values were calculated using pairs of sequences of all vertebrates, mammals or sauropsids nAChRs subunits. (n) Indicates the number of orthologues from each subunit included in the calculations. White background: muscle subunits; light background grey: neuronal subunits; dark grey background : hair cells subunits.

Receptor		α4β2					
Species		Rat		Chicken		Frog	
ACh sensitivity	Mean ± S.E.M (n)	3.11 ± 2.11 (3)	159.76 ± 35.67 (4)	1.07 ± 0.15 (6)	66.00 ± 9.76 (4)	0.75 ± 0.02 (7)	143.71 ± 51.89 (5)
	ANOVA (p-value)	EC50_1: Rat vs Chick = 0.1346, Rat vs Frog = 0.1018, Chick vs Frog = 0.6927^{P}					
		EC50_2: Rat vs Chick = 0.3743, Rat vs Frog = 0.7809, Chick vs Frog = 0.3743^{P}					
Desensitization	Mean ± S.E.M (n)	77.13 ± 1.21 (4)		77.68 ± 5.16 (7)		72.70 ± 3.04 (10)	
	ANOVA (p-value)	Rat vs Chick = 0.9336, Rat vs Frog = 0.7326, Chick vs Frog = 0.7204^{P}					
Ca^{2+} Modulation	Mean ± S.E.M (n)	0.36 ± 0.04 (5)		0.55 ± 0.03 (9)		0.60 ± 0.08 (5)	
	ANOVA (p-value)	Rat vs Chick > 0.999, Rat vs Frog > 0.9999, Chick vs Frog > 0.9999^{P}					
Ca^{2+} Permeability	Mean ± S.E.M (n)	72.07 ± 9.62 (4)		78.75 ± 5.04 (6)		81.51 ± 7.91 (6)	
	ANOVA (p-value)	Rat vs Chick = 0.7999, Rat vs Frog = 0.7892, Chick vs Frog = 0.7999^{P}					
Rectification profile	Mean ± S.E.M (n)	0.07 ± 0.03 (5)		0.03 ± 0.03 (6)		0.02 ± 0.03 (6)	
	ANOVA (p-value)	Rat vs Chick = 0.6838, Rat vs Frog = 0.4995, Chick vs Frog = 0.9437^{P}					

Receptor		α7		
Species		Rat	Chicken	Frog
ACh sensitivity	Mean ± S.E.M (n)	432.1 ± 123.45 (8)	267.56 ± 87.98 (8)	239.27 ± 33.90 (7)
	ANOVA (p-value)	Rat vs Chick = 0.365, Rat vs Frog = 0.6723, Chick vs Frog > 0.9999^{NP}		
Desensitization	Mean ± S.E.M (n)	3.23 ± 0.79 (6)	3.18 ± 0.54 (9)	2.00 ± 0.41 (6)
	ANOVA (p-value)	Rat vs Chick > 0.9999, Rat vs Frog = 0.3743, Chick vs Frog = 0.2496^{NP}		
Ca^{2+} Modulation	Mean ± S.E.M (n)	0.63 ± 0.10 (4)	0.46 ± 0.06 (4)	0.63 ± 0.08 (4)
	ANOVA (p-value)	Rat vs Chick > 0.999, Rat vs Frog > 0.9999, Chick vs Frog > 0.9999^{P}		
Ca^{2+} Permeability	Mean ± S.E.M (n)	29.07 ± 7.68 (4)	37.10 ± 11.82 (4)	38.47 ± 3.98 (7)
	ANOVA (p-value)	Rat vs Chick = 0.7447, Rat vs Frog = 0.7447, Chick vs Frog = 0.8931^{P}		
Rectification profile	Mean ± S.E.M (n)	0.04 ± 0.02 (5)	0.02 ± 0.003 (5)	0.03 ± 0.01 (5)
	ANOVA (p-value)	Rat vs Chick = 0.5909, Rat vs Frog = 0.9706, Chick vs Frog = 0.7295^{P}		

Receptor		α9α10		
Species		Rat	Chicken	Frog
ACh sensitivity	Mean ± S.E.M (n)	19.39 ± 2.08 (9)	17.62 ± 3.33 (6)	110.89 ± 25.00 (7)
	ANOVA (p-value)	Rat vs Chick > 0.9999, Rat vs Frog = 0.0026**, Chick vs Frog = 0.006**^{NP}		
Desensitization	Mean ± S.E.M (n)	64.46 ± 3.65 (5)	60.84 ± 4.23 (9	14.53 ± 3.01 (7)
	ANOVA (p-value)	Rat vs Chick > 0.9999, Rat vs Frog = 0.0051**, Chick vs Frog = 0.0042**^{NP}		
Ca^{2+} Modulation	Mean ± S.E.M (n)	3.76 ± 0.73 (5)	1.00 ± 0.07 (4)	0.63 ± 0.05 (12)
	ANOVA (p-value)	Rat vs Chick < 0.0001****, Rat vs Frog < 0.0001****, Chick vs Frog > 0.9981^{P}		
Ca^{2+} Permeability	Mean ± S.E.M (n)	24.89 ± 2.81 (6)	100.28 ± 14.02 (6)	19.56 ± 3.38 (10)
	ANOVA (p-value)	Rat vs Chick = 0.0299*, Rat vs Frog > 0.9999, Chick vs Frog = 0.0013**^{NP}		
Rectification profile	Mean ± S.E.M (n)	1.21 ± 0.07 (11)	2.31 ± 0.34 (10)	0.21 ± 0.05 (8)
	ANOVA (p-value)	Rat vs Chick = 0.0229*, Rat vs Frog = 0.0406*, Chick vs Frog < 0.0001****^{NP}		

Table 2. Biophysical properties and statistical comparisons from rat, chicken and frog α4β2, α7 and α9α10 receptors. Values are shown as mean ± S.E.M. (n). ^{P}: parametric, ^{NP}: non-parametric analysis. ACh sensitivity: EC_{50} value; Desensitization rate: percentage current remaining 20 seconds (5 sec for α7 receptors) after peak response to a 10-fold concentration of EC_{50} ACh; Ca^{2+} Modulation: current elicited by EC_{50} ACh at Ca^{2+} 0.5 mM relative to Ca^{2+} 3 mM; Ca^{2+} Permeability: percentage of remaining current after BAPTA-AM treatment; Rectification profile: current recorded at +40 mV relative to that recorded at -90 mV.

	PC1	PC2	PC3	PC4	PC5
ACh sensitivity (EC_{50})	0.55	0.04	0.35	0.72	0.23
Desensitization (%*I* after ACh peak)	-0.56	-0.11	-0.35	0.41	0.62
Ca^{2+} modulation ($I_{0.5\ mM}/I_{3\ mM}$)	-0.18	0.77	-0.26	0.36	-0.42
Ca^{2+} permeability (%*I* post-BAPTA)	-0.46	-0.46	0.37	0.38	-0.55
Rectification ($I_{+40\ mV}/I_{-90\ mV}$)	-0.36	0.42	0.74	-0.21	0.31
Proportion of the variability	0.54	0.28	0.14	0.03	0.006
Accumulated proportion	0.54	0.82	0.96	0.99	1.00

Table 3. PCA analysis. *Upper panel*: loading of each experimental parameter on each principal component generated. *Lowe panel*: proportion and accumulated proportion of the variability represented by each PC.

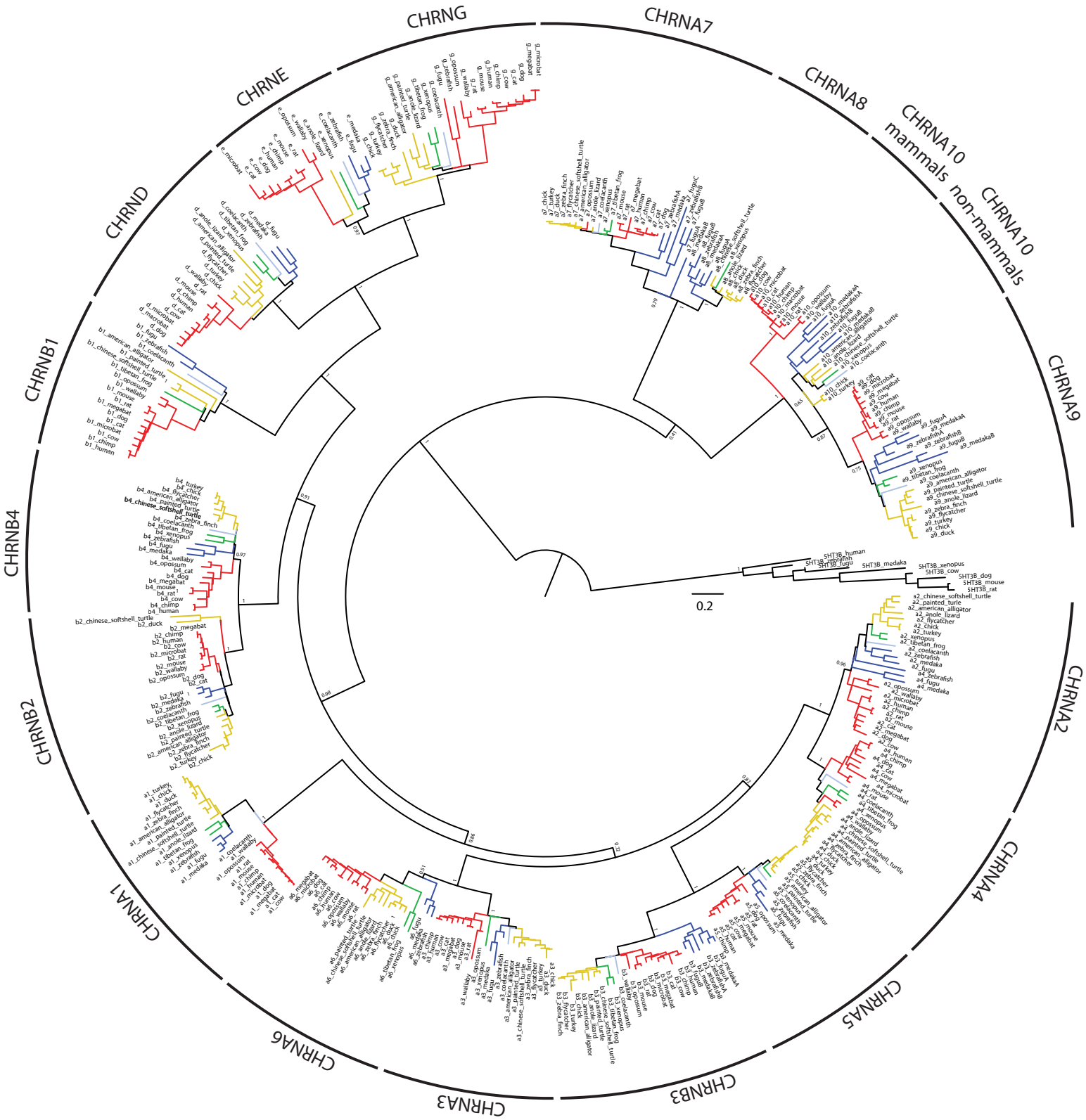

Supplementary Figure 1. Complete minimum evolution phylogenetic tree corresponding to the collapsed tree shown in Figure 1, obtained with variation rates among sites modelled by a gamma distribution. Red branches, mammals; yellow branches, sauropsids; green branches, amphibians; blue branches, fish; light blue branches, coelacanth. The trees were built using minimum evolution method and pairwise deletion for missing sites. The optimal tree with a sum of branch length of 47.32565515 is shown. For clarity, the percentage of replicate trees in which the associated taxa clustered together in the bootstrap test (1,000 replicates) are shown only next to the branches that separate different subunits. The tree is drawn to scale, with branch lengths in the same units as those of the evolutionary distances used to infer the tree.

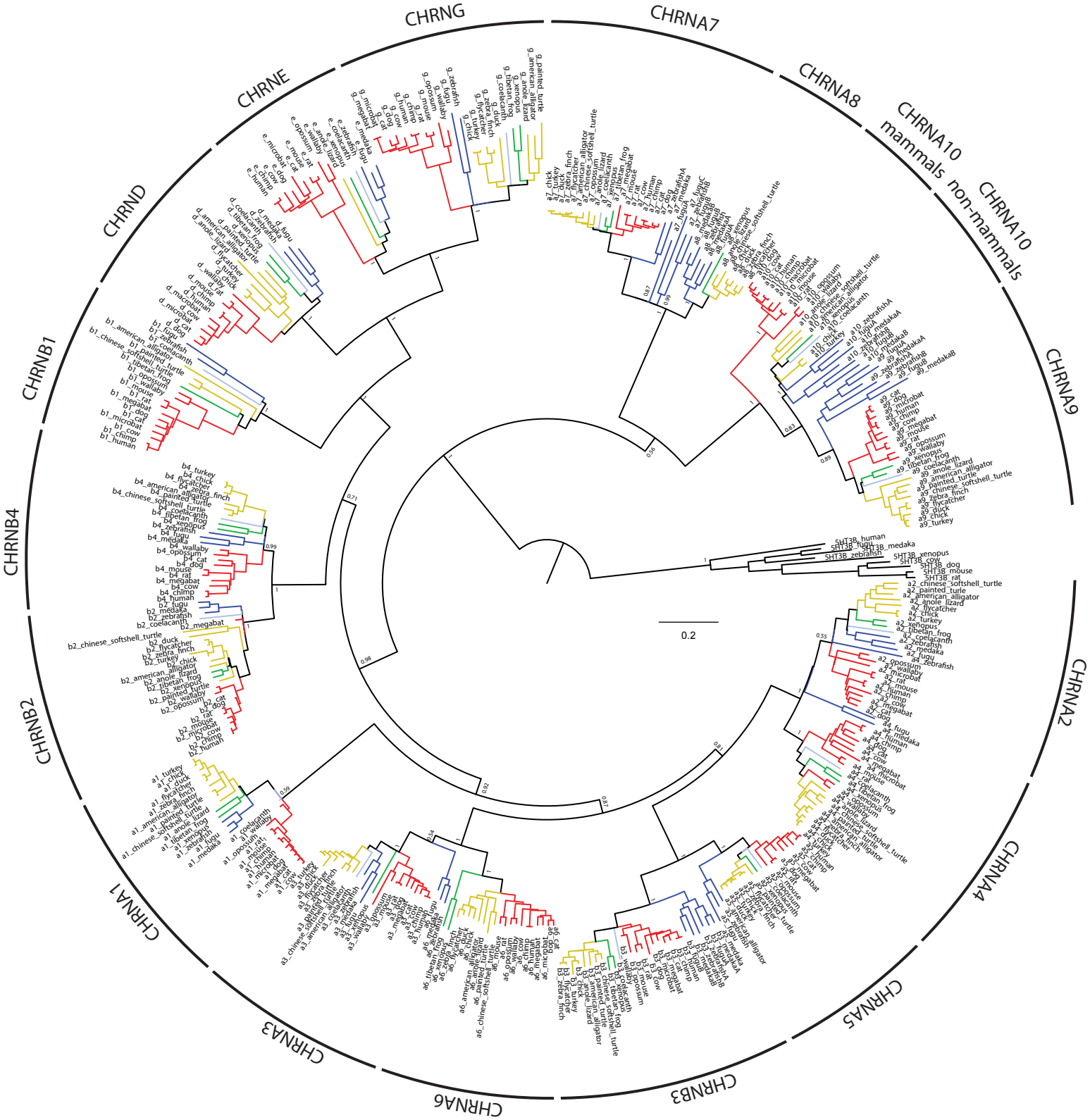

Supplementary Figure 2. Complete minimum evolution phylogenetic tree obtained assuming uniform variation rates among branches. Red branches, mammals; yellow branches, sauropsids; green branches, amphibians; blue branches, fish; light blue branches, coelacanth. The trees were built using minimum evolution method and pairwise deletion for missing sites. The optimal tree with a sum of branch length of 37.49411418 is shown. For clarity, the percentage of replicate trees in which the associated taxa clustered together in the bootstrap test (1,000 replicates) are shown only next to the branches that separate different subunits. The tree is drawn to scale, with branch lengths in the same units as those of the evolutionary distances used to infer the tree.

Supplementary Figure 3. Violin expression plots showing expression level for all nAChR subunits and acetylcholinesterase (AChE) in the different cell types from the datasets analysed. Expression values are in log2 normalised counts (see methods for details).

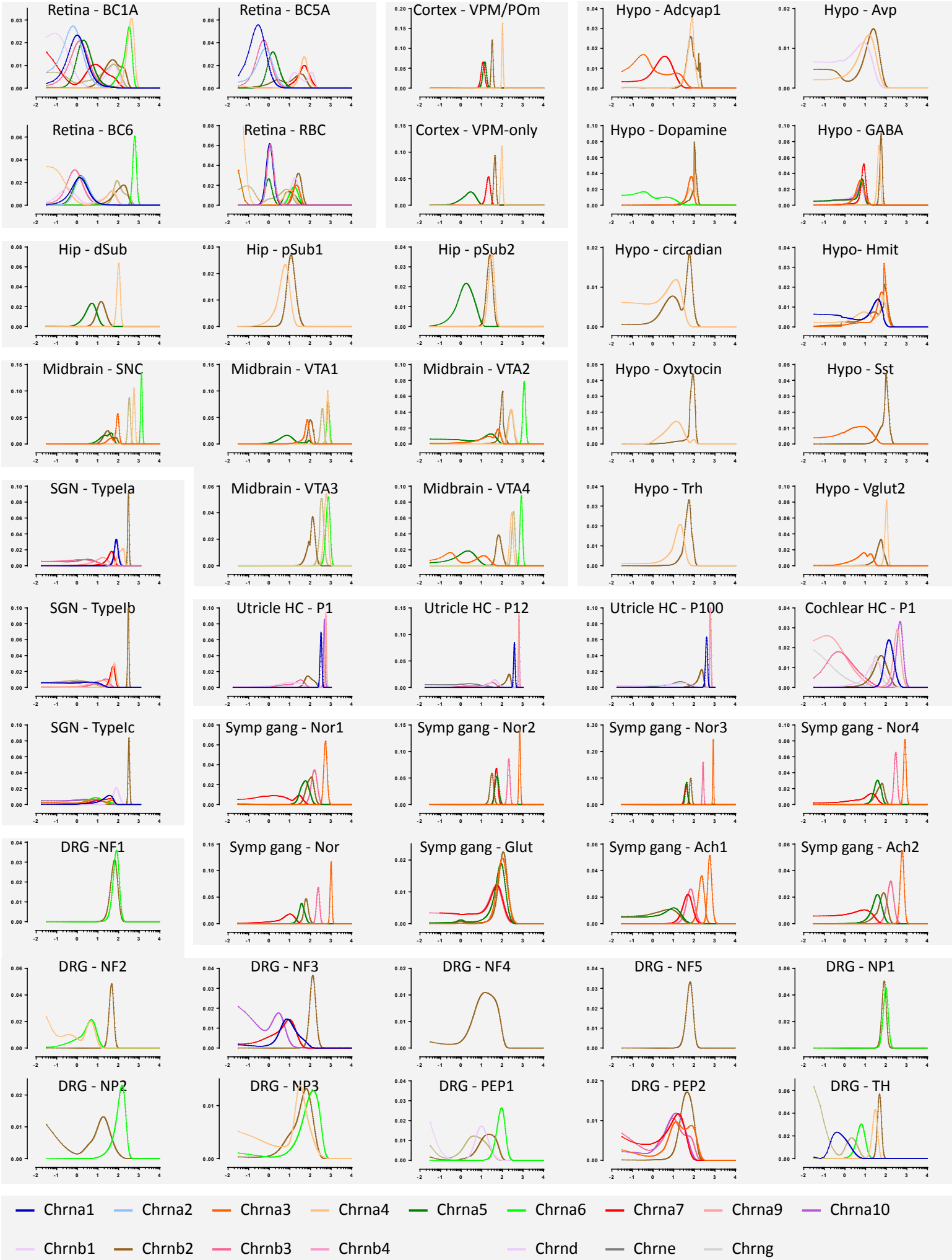

Supplementary Figure 4. Joint posterior probabilities of gene expression levels inferred for the nAChR subunits expressed in the cell types and datasets analysed (see methods for details).

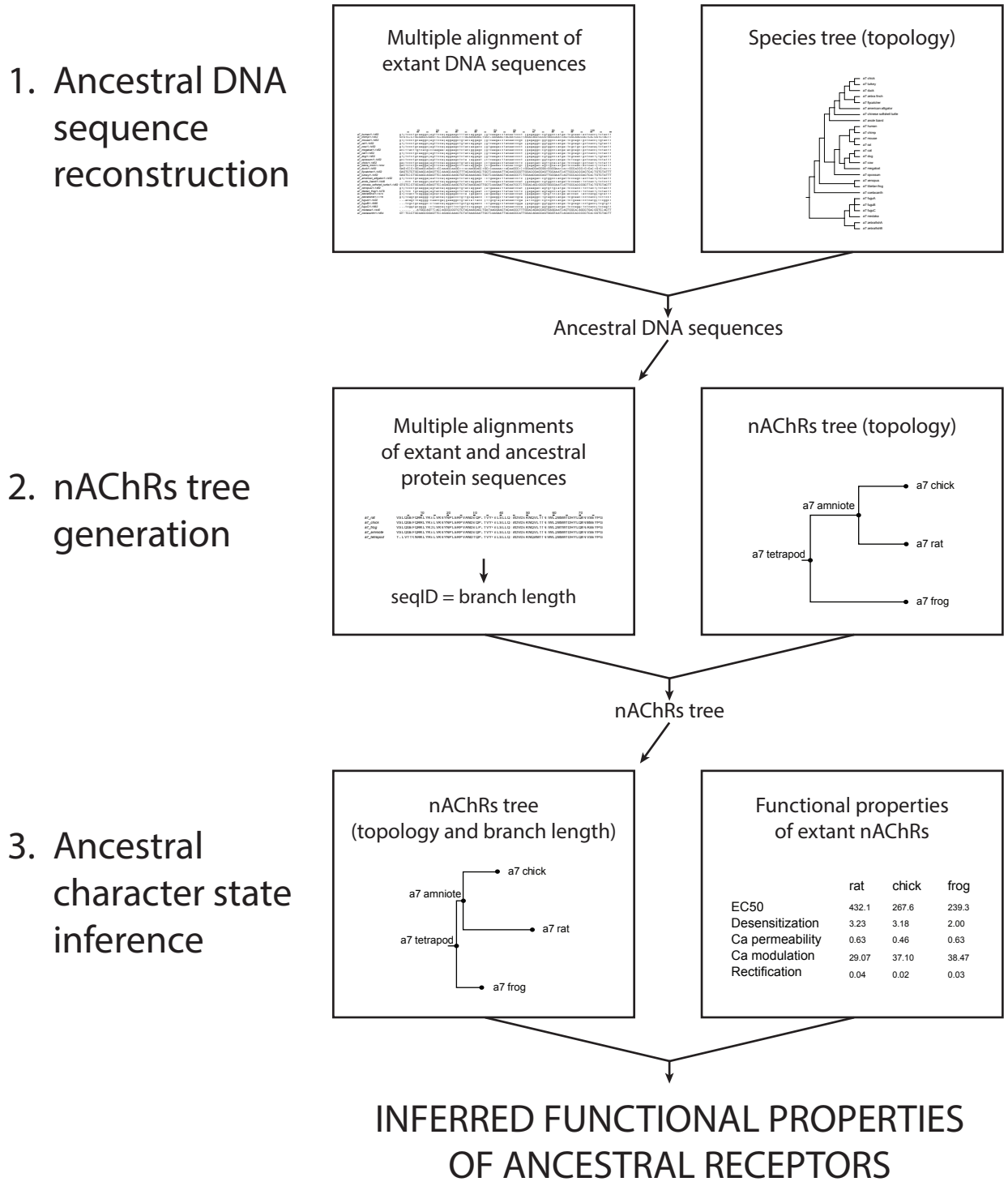

Supplementary Figure 5. Experimental workflow detailing the steps followed for the inference of ancestral character states of the functional properties of tetrapod and amniote ancestral α4β2, α7 and α9α10 receptors.

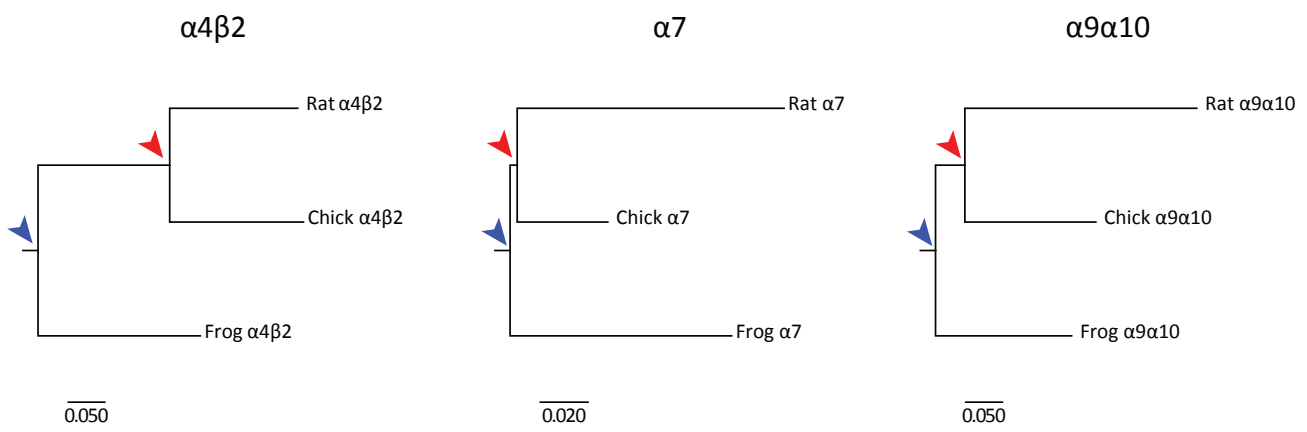

Supplementary Figure 6. nAChRs trees used for the inference of ancestral state states. The tree topology corresponds to the species phylogenetic relationship. The branch lengths correspond to those determined from aminoacid sequence identity analysis between rat-amniote, chick-amniote, amniote-tetrapod and frog-tetrapod pairs of subunits. For the heteromeric α4β2 receptors, branch lengths were calculated assuming a (α4)2(β2)3 assembly. For the heteromeric α9α10 receptors branch lengths were calculated assuming a (α9)2(α10)3 stoichiometry (Plazas et al., 2005). Blue arrows, tetrapod ancestor. Red arrows, amniote ancestor.

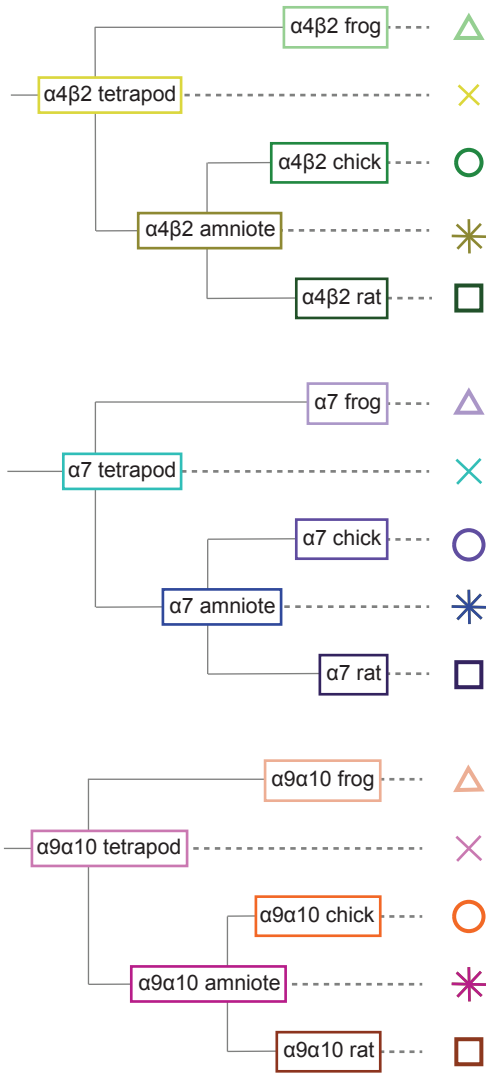

	EC_{50} 1	EC_{50} 2	Desensitization	Ca^{2+} modulation	Ca^{2+} permeability	Rectification
α4β2 frog	0.75	143.71	72.70	0.60	81.51	0.02
α4β2 tetrapod	**1.37**	**130.26**	**74.82**	**0.53**	**78.72**	**0.03**
α4β2 chick	1.07	66.00	77.68	0.55	78.75	0.03
α4β2 amniote	**1.86**	**119.34**	**76.54**	**0.48**	**76.46**	**0.04**
α4β2 rat	3.11	159.76	77.13	0.36	72.07	0.07
α7 frog	239.27		2.00	0.63	38.47	0.03
α7 tetrapod	**291.59**		**2.89**	**0.53**	**35.92**	**0.03**
α7 chick	267.56		3.18	0.46	37.10	0.02
α7 amniote	**293.28**		**2.92**	**0.53**	**35.83**	**0.03**
α7 rat	432.10		3.23	0.63	29.07	0.04
α9α10 frog	110.89		14.53	0.63	19.56	0.21
α9α10 tetrapod	**60.27**		**40.55**	**1.38**	**48.80**	**1.14**
α9α10 chick	17.62		60.84	1.00	100.28	2.31
α9α10 amniote	**49.39**		**46.14**	**1.54**	**55.09**	**1.34**
α9α10 rat	19.39		64.46	3.76	24.89	1.21

Supplementary Figure 7. Inferred ancestral character states for amniote and tetrapod α9α10, α4β2 and α7 nAChRs. The biophysical properties of ancestral receptors inferred by maximum likelihood are shown in black. The values in grey correspond to the biophysical properties of extant receptors determined experimentally (Table 2) and used as input for the inference of ancestral character state. The symbols next to each receptor correspond to the symbols in Figure 8.

	CHRNA1	CHRNA2	CHRNA3	CHRNA4	CHRNA5	CHRNA6	CHRNA7	CHRNA8	CHRNA9	CHRNA10	CHRNB 1	CHRNB 2	CHRNB 3	CHRNB 4	CHRND	CHRNE	CHRNG	5HT3B
Opossum	ENSMODG00000009414	ENSMODG00000015940	ENSMODG00000011883	ENSMODG00000016860	ENSMODG00000011857	ENSMEUG00000010120	ENSMODG00000008920	-	ENSMODG00000020560	ENSMODG00000008246	ENSMODG00000006951	ENSMODG00000017165	ENSMODG00000010082*	ENSMODG00000011891	ENSMODG00000002646*	ENSMODG00000005395	ENSMODG00000002666*	
Wallaby	ENSMEUG00000003627*	ENSMEUG00000004558*	ENSMEUG00000010338*	ENSMEUG00000006728*	-	ENSMEUG00000011281*	ENSMEUG00000009840*	-	ENSMEUG00000010143*	ENSMEUG00000009564*	ENSMEUG00000008924*	ENSMEUG00000003725*	ENSMEUG00000011355*	ENSMEUG00000001043*	ENSMEUG00000011484*	ENSMEUG00000012185*	ENSMEUG00000011510*	
Rat	ENSRNOG00000018286	ENSRNOG00000017424	ENSRNOG00000013829	ENSRNOG00000011202	ENSRNOG00000013610	ENSRNOG00000012283	ENSRNOG00000010853	-	ENSRNOG00000002484	ENSRNOG00000020293	ENSRNOG00000014698	ENSRNOG00000020778	ENSRNOG00000012448	ENSRNOG00000014427	ENSRNOG00000019527	ENSRNOG00000003777	NM_019145.1	
Mouse	ENSMUSG00000027107	ENSMUSG00000022041	ENSMUSG00000032303	ENSMUSG00000027577	ENSMUSG00000035594	ENSMUSG00000031491	ENSMUSG00000030525	-	ENSMUSG00000029205	ENSMUSG00000066279	ENSMUSG00000041189	ENSMUSG00000027950	ENSMUSG00000031492	ENSMUSG00000035200	ENSMUSG00000026251	ENSMUSG00000014609	ENSMUSG00000026253	ENSMUSG00000008590
Cat	ENSFCAG00000014103*	ENSFCAG00000028158	ENSFCAG00000001932	ENSFCAG00000030656	ENSFCAG00000001930	ENSFCAG00000022358	ENSFCAG00000036300	-	ENSFCAG00000035547	ENSFCAG00000023105	ENSFCAG00000009612	ENSFCAG00000022169*	ENSFCAG00000010080	ENSFCAG00000001933	ENSFCAG00000030943	ENSFCAG00000038719	ENSFCAG00000005681	ENSFCAG00000004982
Dog	ENSCAFG00000013283	ENSCAFG00000008499	ENSCAFG00000001710*	ENSCAFG00000012893	ENSCAFG00000001745*	ENSCAFG00000005444	ENSCAFG00000010220*	-	ENSCAFG00000015915	ENSCAFG00000024527	ENSCAFG00000016315	ENSCAFG00000017172	ENSCAFG00000005460	ENSCAFG00000023904	ENSCAFG00000011283	ENSCAFG00000015838	ENSCAFG00000024807*	ENSCAFG00000013576
Cow	ENSBTAG00000018253	ENSBTAG00000002252	ENSBTAG00000003130	ENSBTAG00000017198	ENSBTAG00000013657*	ENSBTAG00000014056	ENSBTAG00000015775	-	ENSBTAG00000015252	ENSBTAG00000055237	ENSBTAG00000019242	ENSBTAG00000007517	ENSBTAG00000014050	ENSBTAG00000003132	ENSBTAG00000011390*	ENSBTAG00000004908	ENSBTAG00000045943	ENSBTAG00000031330
Human	ENSG00000138435	ENSG00000120903	ENSG00000080644	ENSG00000101204	ENSG00000016984	ENSG00000147434	ENSG00000175344	-	ENSG00000174343	ENSG00000129749	ENSG00000170175	ENSG00000160716	ENSG00000147432	ENSG00000117971	ENSG00000135902	ENSG00000108556	ENSG00000196811	ENSG00000149305
Chimp	ENSPTRG00000012658	ENSPTRG00000020105	ENSPTRG00000007347	ENSPTRG00000013735	ENSPTRG00000007346	ENSPTRG00000020210	ENSPTRG00000006865	-	ENSPTRG00000016003	ENSPTRG00000003199	ENSPTRG00000008689	ENSPTRG00000001389	ENSPTRG00000020209	ENSPTRG00000007348	ENSPTRG00000013040	ENSPTRG00000008612	ENSPTRG00000022726	
Megabat	ENSPVAG00000004164	ENSPVAG00000014424	ENSPVAG00000009191	ENSPVAG00000014109	ENSPVAG00000009186	ENSPVAG00000015371*	ENSPVAG00000017796*	-	ENSPVAG00000003814	ENSPVAG00000016436	ENSPVAG00000005067	XM_023534307.1*	ENSPVAG00000015373	ENSPVAG00000009193	ENSPVAG00000007491	ENSPVAG00000000127	ENSPVAG00000007492*	
Microbat	ENSMLUG00000015698	ENSMLUG00000001512	-	Manual search on traces	-	ENSMLUG00000005231	ENSMLUG00000005856	-	ENSMLUG00000000893	ENSMLUG00000013586	ENSMLUG00000009921	ENSMLUG00000007541	ENSMLUG00000027322	-	ENSMLUG00000011213	ENSMLUG00000015682*	ENSMLUG00000011237	
Chick	ENSGALG00000009301	ENSGALG00000016565	ENSGALG00000003014	ENSGALG00000005801	ENSGALG00000003021	ENSGALG00000015382	ENSGALG00000004096	ENSGALG00000015336	ENSGALG00000014268	NM_001101036.1	-	ENSGALG00000002707	ENSGALG00000015384	ENSGALG00000003005	ENSGALG00000007899	-	ENSGALG00000007906	
Turkey	ENSMGAG00000009752	ENSMGAG00000014105	ENSMGAG00000003578	ENSMGAG00000006295	ENSMGAG00000003610*	-	ENSMGAG00000005132	-	ENSMGAG00000012228	XM_010706263.2	-	ENSMGAG00000006636*	ENSMGAG00000007510	ENSMGAG00000003559*	ENSMGAG00000008354	-	ENSMGAG00000008414	
Duck	ENSAPLG00000007803*	ENSAPLG00000009491*	ENSAPLG00000016121	ENSAPLG00000007776	ENSAPLG00000016223*	ENSAPLG00000012469	ENSAPLG00000010434	ENSAPLG00000007724	ENSAPLG00000013711*	-	-	ENSAPLG00000009547*	ENSAPLG00000012846	ENSAPLG00000016042	-	-	ENSAPLG00000015469*	
Flycatcher	ENSFALG00000003034	ENSFALG00000003731	ENSFALG00000010658	ENSFALG00000010418	ENSFALG00000010653	ENSFALG00000005209	ENSFALG00000012362*	ENSFALG00000001025	ENSFALG00000002853*	XM_016305564.1	-	ENSFALG00000001220	ENSFALG00000005194	ENSFALG00000010665	ENSFALG00000007740	-	ENSFALG00000007743	
Zebra finch	ENSTGUG00000008827	-	ENSTGUG00000003469	ENSTGUG00000007453	ENSTGUG00000003451*	ENSTGUG00000000216*	ENSTGUG00000005850	ENSTGUG00000000135	ENSTGUG00000008712	-	-	ENSTGUG00000004092	ENSTGUG00000000227	XM_002191803.3	-	-	ENSTGUG00000009924	
Anole lizard	ENSACAG00000005293	ENSACAG00000002388	-	ENSACAG00000005817	-	ENSACAG00000005512	ENSACAG00000008436	ENSACAG00000005448	ENSACAG00000011789	NW_003340045.1	-	ENSACAG00000015594	ENSACAG00000005630	-	ENSACAG00000010984	ENSACAG00000014790*	ENSACAG00000010910	
American alligator	XM_006267516.3	XM_006274660.2	XM_006261354.3	XM_019484414.1	XM_006261353.3	XM_006276967.2	XM_014599894.2	-	XM_019478038.1	XM_019480144.1	XM_006275274.2	XM_019497730	XM_006276963.2	XM_014605947	XM_019484776.1	-	NW_017709597.1*	
Chinese softshell turtle	ENSPSIG00000003348	ENSPSIG00000012597	ENSPSIG00000016882	ENSPSIG00000012045	-	ENSPSIG00000006517	ENSPSIG00000010525	ENSPSIG00000009608	ENSPSIG00000017539	XM_014580618.2	ENSPSIG00000009407	ENSPSIG00000006807*	ENSPSIG00000017586*	ENSPSIG00000017214	-	ENSPSIG00000003627*	ENSPSIG00000011304*	
Painted turtle	ENSCPBG00000003798	ENSCPBG00000022315	ENSCPBG00000024258	ENSCPBG00000027193	ENSCPBG00000024257	ENSCPBG00000027581*	-	-	ENSPSIG00000017539*	XM_024109380.1	ENSCPBG00000004679	ENSCPBG00000024641*	ENSCPBG00000027579	ENSCPBG00000024259	ENSCPBG00000016193	ENSCPBG00000016561*	ENSCPBG00000016190	
Xenopus tropicalis	ENSXETG00000025420	ENSXETG00000017553	ENSXETG00000031723	ENSXETG00000023746	ENSXETG00000023896*	ENSXETG00000010249*	ENSXETG00000016395	ENSXETG00000018003	ENSXETG00000012803	XM_002942872.4	-	ENSXETG00000003846	ENSXETG00000010250	ENSXETG00000033968*	ENSXETG00000027884	ENSXETG00000014957	ENSXETG00000013994*	ENSXETG00000031022
Tibetan frog	XM_018572442.1	XM_018570301.1	-	XM_018560101.1	-	XM_018557911.1	XM_018564234.1	-	XM_018564438.1	-	XM_018573841.1	XM_018570082.1	XM_018557907.1	XM_018572684.1	XM_018563344.1	-	XM_018572139.1	
Coelacanth	ENSLACG00000000109*	ENSLACG00000003345	XM_006001841.1	ENSLACG00000010383*	ENSLACG00000002798	-	ENSLACG00000005760*	-	ENSLACG00000009570	ENSLACG00000005922	ENSLACG00000008409	ENSLACG00000015217	ENSLACG00000002288	ENSLACG00000004838*	ENSLACG00000015676	ENSLACG00000002691	ENSLACG00000015771	
Fugu	XM_003961904.2	ENSTRUG00000008002*	ENSTRUG00000004067*	ENSTRUG00000010213	ENSTRUG00000005757	ENSTRUT00000002729.2	ENSTRUG00000016472	ENSTRUG00000002223	ENSTRUG00000010253	ENSTRUG00000003807	XM_011618734.1	ENSTRUG00000005762	ENSTRUG00000006363	ENSTRUG00000025609	ENSTRUG00000007767*	ENSTRUG00000016224	ENSTRUG00000014376*	ENSTRUG00000013084
						ENSTRUT00000016710.2	NC_018902.1	ENSTRUG00000005961	ENSTRUG00000013071	NW_004072435.1			ENSTRUG00000001764					
							NC_018896.1											
Medaka	XM_020713072.2	XM_011491375.3	ENSORLG00000013118	ENSORLG00000000865*	ENSORLG00000020077	ENSORLT00015028636.1	ENSORLG00000018774	ENSORLG00000003203	ENSORLG00000004390	NC_019871.2	-	ENSORLG00000009700	ENSORLG00000003226	ENSORLG00000013114	ENSORLG00000026994	ENSORLG00000008035*	-	ENSORLG00000014619
							ENSORLG00000030549	ENSORLG00000014282	ENSORLG00000005701	XM_011483838.3			ENSORLG00000014290					
Zebrafish	ENSDARG00000009021	NM_001040327.1	ENSDARG00000100991	NM_001048063.1	ENSDARG00000003420	ENSDARG00000055559	ENSDARG00000101522	ENSDARG00000087224	ENSDARG00000054680	NM_001044804.1	NM_001253810.1	ENSDARG00000017790	ENSDARG00000052764	ENSDARG00000101677	ENSDARG00000019342	ENSDARG00000034307	ENSDARG00000086647*	ENSDARG00000061749
							ENSDARG00000101702		ENSDARG00000099181	XM_021481417.1			ENSDARG00000038508					

Supplementary Table 1. Accession numbers for sequences used in the phylogenetic analysis. Accession numbers correspond to Ensembl or Genbank databases. * Sequences mended and/or completed using trace fragments obtained from the NCBI Genome Project traces database.

nAChR subtype	DOI	Reference
α7	10.1016/0896-6273(90)90344-F	Couturier et al., 1990
α8	PMID: 7509438	Gerzanich et al., 1994
α9	10.1016/0092-8674(94)90555-X	Elgoyhen 1994 et al., 1994
α10	10.1093/molbev/msu258	Lipovsek et al., 2014
α2β2	10.1016/0896-6273(88)90208-5	Deneris et al., 1988
α2β4	10.1016/0896-6273(89)90207-9	Duvoisin et al.,1989
α3β2	10.1073/pnas.84.21.7763	Boulter et al., 1987
α3β4	10.1016/0896-6273(89)90207-9	Duvoisin et al.,1989
α4β2	10.1073/pnas.84.21.7763	Boulter et al., 1987
α4β4	10.1016/0896-6273(89)90207-9	Duvoisin et al., 1989
α6β2	10.1046/j.1460-9568.1998.00001.x	Fucile et al., 1998
α6β4	10.1124/mol.106.027326	Tumkosit et al., 2006
α7β2	10.1113/jphysiol.2001.013847	Khiroug et al., 2002
α7β3	10.1074/jbc.274.26.18335	Palma etal., 1999
α7β4	110.1111/j.1471-4159.2012.07931.x	Criado et al., 2012
α9α10	10.1073/pnas.051622798	Elgoyhen et al., 2001
α2α5β2	10.1124/mol.63.6.1329	Vailati et al., 2003
α2α6β2	10.1124/mol.105.015925	Gotti et al., 2005
α2β2β3	10.1111/j.1471-4159.2012.07685.x	Dash et al., 2012
α2β3β4	10.1111/j.1471-4159.2012.07685.x	Dash et al., 2012
α3α4β2	10.1523/JNEUROSCI.2112-05.2005	Turner et al., 2005
α3α4β4	10.1523/JNEUROSCI.2112-05.2005	Turner et al., 2005
α3α5β2	10.1074/jbc.271.30.17656	Wang et al., 1996
α3α5β4	10.1074/jbc.271.30.17656	Wang et al., 1996
α3α6β2	10.1016/S0028-3908(00)00144-1	Kuryatov et al., 2000
α3α6β4	10.1046/j.1460-9568.1998.00001.x	Fucile et al., 1998
α3β2β4	10.1523/JNEUROSCI.2112-05.2005	Turner et al., 2005
α3β2β3	10.1111/j.1471-4159.2012.07685.x	Dash et al., 2012
α3β3β4	10.1074/jbc.273.25.15317	Groot-Kormelink et al., 1998
α4α5β2	10.1038/380347a0	Ramirez-Latorre et al., 1996
α4β2β3	10.1124/mol.108.046789	Kuryatov et al., 2008
α4β3β4	10.1111/j.1471-4159.2012.07685.x	Dash et al., 2012
α5α6β2	10.1016/S0028-3908(00)00144-1	Kuryatov et al., 2000
α5α7β2	10.1111/j.1749-6632.1999.tb11331.x	Girod et al., 1999
α6β2β3	10.1124/mol.106.027326	Tumkosit et al., 2006
α6β3β4	10.1016/S0028-3908(00)00144-1	Kuryatov et al., 2000
α3α4α6β2	10.1111/j.1471-4159.2008.05282.x	Cox etal., 2008
α3α5β2β4	10.1074/jbc.270.9.4424	Conroy and Berg, 1995
α4α6β2β3	10.1124/mol.110.066159	Kuryatov and Lindstrom, 2010
α5α6β3β4	10.1124/jpet104.075069	Grinevich et al., 2005
α1β1γδ	10.1038/321406a0	Mishina et al., 1986
α1β1δε	10.1038/321406a0	Mishina et al., 1986

Supplementary Table 2. Neuronal nAChRs repertoire. Experimentally validated pentameric combinations of nAChR subunits and relevant literature references.

Publication	DOI	Accession	Tissue	mean_genes	Cell_types	#Cells
Shekar, et al. 2016	10.1016/j.cell.2016.07.054	GSE81905	Retina	5372	BC1A	14
					BC5A	24
					BC6	17
					RBC	99
Chevee, et al. 2018	10.1016/j.celrep.2017.12.046	GSE107632	Somatosensory cortex	5614	VPMonly	130
					VPM/Pom	210
Cembrowski, et al. 2018	10.1016/j.cell.2018.03.031	GSE100449	Hippocampus	5218	dSub	72
					pSub1	69
					pSub2	102
Romanov	10.1038/nn.4462	GSE74672	Hypothalamus	3887	Adcyap1	34
					Avp	25
					Dopamine	41
					GABA	311
					circadian	31
					Hmit	24
					Oxytocin	37
					Sst	38
					Trh	55
					Vglut2	137
LaManno, et al. 2016	10.1016/j.cell.2016.09.027	GSE76381	Ventral midbrain	4106	DA_SNC	73
					DA_VTA1	47
					DA_VTA2	28
					DA_VTA3	26
					DA_VTA4	69
Shrestha, et al. 2018	10.1016/j.cell.2018.07.007	GSE114997	Spiral ganglion	8298	SGN_TypeIa	63
					SGN_TypeIb	71
					SGN_TypeIc	45
McInturff	10.1242/bio.038083	GSE115934.	utricle HC	5578	HC_P1	37
					HC_P12	50
					HC_P100	25
Burns	10.1038/ncomms9557	GSE71982	inner ear	7143	Co_HC	10
Furlan, et al. 2016	10.1038/nn.4376	GSE78845	Sympathetic ganglion	6297	Nor1	10
					Nor2	39
					Nor3	103
					Nor4	18
					Nor5	23
					Glu	4
					Ach1	8
					Ach2	8
Usoskin	10.1038/nn.3881	GSE59739	DRG	3821	NF1	21
					NF2	43
					NF3	10
					NF4	16
					NF5	24
					NP1	80
					NP2	19
					NP3	10
					PEP1	50
					PEP2	14
					TH	142

Supplementary Table 3. Single-cell RNA sequencing datasets. Accession information for the datasets used on the analysis of nAChR subunits co-expression patterns. mean_genes, average number of genes per cell detected in each dataset. Cell_types, final cell types, as inferred in each publication, used to estimate the expression levels of nAChR subunit genes. #Cells, number of cells for each cell type present in the final datasets analysed.

	Retina				Somatosensory cortex		Hippocampus			Hypothalamus									
	BC1A	BC5A	BC6	RBC	VPM-only	VPM/Pom	dSub	pSub1	pSub2	Adcyap1	Avp	Dopamine	GABA	circadian	Hmit	Oxytocin	Sst	Trh	Vglut2
Chrna1	3.46	0.72	3.18	1.24	0.00	0.00	0.00	0.00	0.00	0.00	0.00	0.00	0.00	0.00	24.85	0.00	0.00	0.00	0.00
Chrna2	2.93	1.41	3.17	1.37	0.00	0.00	0.00	0.00	0.00	0.00	0.00	0.00	0.00	0.00	0.00	0.00	0.00	0.00	0.00
Chrna3	0.00	0.00	0.00	13.35	0.00	0.00	0.00	0.00	0.00	8.33	0.00	62.03	5.92	0.00	59.68	0.00	8.54	0.00	9.97
Chrna4	382.03	52.93	25.66	6.74	92.58	100.99	99.88	6.10	30.51	68.76	14.87	80.34	43.55	10.23	37.64	17.36	0.00	17.47	100.82
Chrna5	5.35	2.48	3.18	8.01	3.05	13.80	5.36	0.00	2.68	0.00	0.00	0.00	4.89	0.00	0.00	0.00	0.00	0.00	0.00
Chrna6	267.64	0.00	601.04	10.78	0.00	0.00	0.00	0.00	0.00	0.00	0.00	5.67	0.00	0.00	0.00	0.00	0.00	0.00	0.00
Chrna7	19.29	52.13	0.00	0.00	20.54	11.37	0.00	0.00	0.00	5.39	0.00	0.00	7.56	0.00	0.00	0.00	0.00	0.00	0.00
Chrna9	0.00	0.00	0.00	0.00	0.00	0.00	0.00	0.00	0.00	0.00	0.00	0.00	0.00	0.00	0.00	0.00	0.00	0.00	0.00
Chrna10	0.88	0.00	0.00	0.00	0.00	0.00	0.00	0.00	0.00	0.00	0.00	0.00	4.53	0.00	0.00	0.00	0.00	0.00	0.00
Chrnb1	34.77	55.02	28.26	17.92	0.00	0.00	0.00	0.00	0.00	0.00	8.59	0.00	3.98	0.00	0.00	0.00	0.00	0.00	0.00
Chrnb2	78.90	23.43	134.51	25.77	43.13	31.83	15.83	13.12	24.99	83.16	21.37	99.08	55.77	35.06	53.54	75.05	92.14	50.69	79.18
Chrnb3	43.53	0.46	138.25	5.91	0.00	0.00	0.00	0.00	0.00	0.00	0.00	0.00	4.86	0.00	0.00	0.00	0.00	0.00	0.00
Chrnb4	4.68	1.14	2.02	1.33	0.00	0.00	0.00	0.00	0.00	0.00	0.00	0.00	0.00	0.00	0.00	0.00	0.00	0.00	0.00
Chrnd	0.00	0.00	0.00	0.00	0.00	0.00	0.00	0.00	0.00	0.00	0.00	0.00	0.00	0.00	0.00	0.00	0.00	0.00	0.00
Chrne	0.00	0.00	0.00	0.00	0.00	0.00	0.00	0.00	0.00	0.00	0.00	0.00	0.00	0.00	0.00	0.00	0.00	0.00	0.00
Chrng	0.00	0.00	0.00	0.00	0.00	0.00	0.00	0.00	0.00	0.00	0.00	0.00	0.00	0.00	0.00	0.00	0.00	0.00	0.00

	Ventral midbrain					Spiral ganglion			Inner ear hair cells			
	SNC	VTA1	VTA2	VTA3	VTA4	TypeIa	TypeIb	TypeIc	Utricle_HC_P1	Utricle_HC_P12	Utricle_HC_P100	Cochlear_HC
Chrna1	0.00	0.00	0.00	0.00	0.00	76.33	5.52	27.55	320.99	376.92	388.80	154.91
Chrna2	0.00	0.00	0.00	0.00	0.00	0.00	0.00	0.00	0.00	0.00	0.00	0.00
Chrna3	75.04	61.02	34.75	0.00	9.22	0.00	0.00	16.67	0.00	0.00	0.00	0.00
Chrna4	559.44	674.74	277.56	568.53	274.87	131.75	57.37	18.66	0.00	0.00	0.00	0.00
Chrna5	28.65	16.99	19.36	0.00	3.32	0.00	0.00	0.00	0.00	0.00	0.00	0.00
Chrna6	1286.75	718.59	1140.92	705.52	821.02	0.00	0.00	11.64	0.00	0.00	0.00	0.00
Chrna7	0.00	0.00	0.00	0.00	0.00	37.61	49.86	21.04	0.00	0.00	0.00	0.00
Chrna9	0.00	0.00	0.00	0.00	0.00	15.33	13.61	0.00	554.41	626.98	607.56	350.02
Chrna10	0.00	0.00	0.00	0.00	0.00	0.00	4.42	7.33	464.02	632.15	599.18	466.89
Chrnb1	0.00	0.00	0.00	0.00	0.00	80.87	59.75	76.27	15.00	39.59	26.26	39.70
Chrnb2	37.12	100.00	91.58	117.53	70.01	298.16	295.47	315.08	96.02	175.77	182.60	62.75
Chrnb3	326.52	370.87	260.30	351.18	344.16	0.00	3.64	11.32	0.00	0.00	0.00	0.00
Chrnb4	0.00	0.00	0.00	0.00	0.00	4.39	18.07	0.00	24.11	22.30	2.31	4.21
Chrnd	0.00	0.00	0.00	0.00	0.00	0.00	0.00	0.00	0.00	0.00	0.00	2.35
Chrne	0.00	0.00	0.00	0.00	0.00	4.97	5.00	7.81	0.00	5.92	22.78	0.00
Chrng	0.00	0.00	0.00	0.00	0.00	0.00	0.00	0.00	509.75	40.42	0.00	32.97

	Visceral motor neurons								Dorsal root ganglia										
	Nor1	Nor2	Nor3	Nor4	Nor5	Glut	Ach1	Ach2	NF1	NF2	NF3	NF4	NF5	NP1	NP2	NP3	PEP1	PEP2	TH
Chrna1	0.00	0.00	0.00	0.00	0.00	0.00	0.00	0.00	0.00	0.00	15.18	0.00	0.00	0.00	0.00	0.00	0.00	0.00	0.79
Chrna2	0.00	0.00	0.00	0.00	0.00	0.00	0.00	0.00	0.00	0.00	0.00	0.00	0.00	0.00	0.00	0.00	0.00	0.00	0.00
Chrna3	535.34	689.45	825.02	808.62	988.48	107.72	572.22	596.98	0.00	0.00	0.00	0.00	0.00	0.00	0.00	0.00	0.00	40.86	0.00
Chrna4	0.00	0.00	0.00	0.00	0.00	0.00	9.93	0.00	0.00	3.45	0.00	0.00	0.00	0.00	0.00	44.71	0.00	0.00	28.78
Chrna5	55.99	50.79	41.92	38.86	38.83	0.00	51.51	37.33	0.00	0.00	0.00	0.00	0.00	0.00	0.00	0.00	0.00	0.00	0.00
Chrna6	0.00	0.00	0.00	0.00	0.00	79.15	0.00	0.00	76.83	4.69	0.00	0.00	0.00	95.66	128.57	126.53	89.34	0.00	6.40
Chrna7	12.13	30.63	39.57	15.58	9.06	0.00	0.00	8.86	0.00	0.00	9.14	0.00	0.00	0.00	0.00	0.00	0.00	15.08	0.00
Chrna9	0.00	0.00	0.00	0.00	0.00	0.00	0.00	0.00	0.00	0.00	0.00	0.00	0.00	0.00	0.00	0.00	0.00	0.00	0.00
Chrna10	0.00	0.00	0.00	0.00	0.00	0.00	0.00	0.00	0.00	0.00	3.03	0.00	0.00	0.00	0.00	0.00	0.00	17.27	0.00
Chrnb1	0.00	0.00	0.00	0.00	0.00	0.00	7.76	0.00	0.00	0.00	0.00	0.00	0.00	0.00	0.00	0.00	11.97	0.00	0.00
Chrnb2	90.59	50.45	60.37	46.26	56.20	42.76	62.82	61.41	62.69	45.23	134.24	25.43	61.54	79.49	21.35	59.17	25.69	50.66	47.42
Chrnb3	0.00	0.00	0.00	0.00	0.00	109.59	0.00	0.00	0.00	0.00	0.00	0.00	0.00	4.15	0.00	0.00	9.39	0.00	1.70
Chrnb4	154.87	202.31	264.13	290.53	232.07	42.76	222.23	164.63	0.00	0.00	0.00	0.00	0.00	1.81	0.00	0.00	0.00	23.00	0.00
Chrnd	0.00	0.00	0.00	0.00	0.00	0.00	0.00	0.00	0.00	0.00	0.00	0.00	0.00	0.00	8.76	0.00	0.00	0.00	0.00
Chrne	0.00	0.00	0.00	0.00	0.00	0.00	0.00	0.00	0.00	0.00	0.00	0.00	0.00	0.00	0.00	0.00	0.00	0.00	0.00
Chrng	0.00	0.00	0.00	0.00	0.00	0.00	0.00	0.00	0.00	0.00	0.00	0.00	0.00	0.00	0.00	0.00	0.00	0.00	0.00

Supplementary Table 4. Mean expression of nAChR subunits genes across cell types. Values are means of the estimated joint posterior distributions of gene expression levels inferred for the nAChR subunits expressed in the cell types and datasets analysed.

Primer	Tm (ºC)	Sequence (5'-3')
FXtrop.a9	61.4	TA**GAATTC**ATGCACACATTTTTGGCACGTGTTGG
RXtrop.a9	63.1	AT**CTCGAG**TCACACTGCCTGGGCAATAA
FXtrop.a10	62.4	AT**AAGCTT**TCCTGCCCAACATGAGACTGC
RXtrop.a10	62.1	AT**CTCGAG**GGCACCATCATATGGCTTTG
FXtrop.a7	61.8	TA**GAATTC**TTTGATCTCCTGCGATGGGAGGA
RXtrop.a7	61.9	AT**CTCGAG**TAGAACTGCAGAACCCTAAGCAA
FXtrop.a4	62.7	AT**GAATTC**GCTCTCTGCCAACATGGGTG
RXtrop.a4	60.1	TA**AAGCTT**GGGGTCAGTTCATATCAAACCAG
FXtrop.b2	61.2	TA**GAATTC**GAGGCGATGAGATGATCCGG
RXtrop.b2	61.3	AT**CTCGAG**GCCCTCAATGTTTCTCAGTT

Supplementary Table 5. Primers used for the cloning of *X. tropicalis* nAChRs subunits. The restriction sites for EcoRI, XhoI and HindIII used for subsequent subcloning are highlighted in bold. Tm, annealing temperature.

Receptor	ACh sensitivity (EC_{50})	Desensitization (%*I* after ACh peak)	Ca^{2+} modulation ($I_{0.5\ mM}/I_{3\ mM}$)	Ca^{2+} permeability (%*I* post-BAPTA)	Rectification ($I_{+40\ mV}/I_{-90\ mV}$)
Rat α9α10	0.045	0.830	1.000	0.248	0.525
Chick α9α10	0.041	0.783	0.266	1.000	1.000
Frog α9α10	0.257	0.187	0.167	0.195	0.091
Rat α4β2	0.007	0.993	0.097	0.719	0.029
Chick α4β2	0.002	1.000	0.146	0.785	0.014
Frog α4β2	0.002	0.936	0.158	0.813	0.008
Rat α7	1.000	0.042	0.167	0.290	0.016
Chick α7	0.619	0.041	0.121	0.370	0.009
Frog α7	0.554	0.026	0.168	0.384	0.015
Amniote α4β2	0.004	0.985	0.128	0.762	0.019
Tetrapod α4β2	0.003	0.963	0.141	0.785	0.014
Amniote α7	0.679	0.038	0.141	0.357	0.012
Tetrapod α7	0.675	0.037	0.142	0.358	0.012
Amniote α9α10	0.114	0.594	0.409	0.549	0.581
Tetrapod α9α10	0.139	0.522	0.366	0.487	0.494

Supplementary Table 6. Normalized biophysical properties from extant and normalised inferred biophysical properties for ancestral receptors used in PCA analysis. Values are normalised relative to the maximum obtained for each parameter.

α4β2		
Comparison	**seqID**	**1-seqID**
Rat-amniote	0.824	0.176
Chick-amniote	0.816	0.184
Amniote-tetrapod	0.819	0.181
Frog-tetrapod	0.777	0.223

α7		
Comparison	**seqID**	**1-seqID**
Rat-amniote	0.888	0.112
Chick-amniote	0.962	0.038
Amniote-tetrapod	0.997	0.003
Frog-tetrapod	0.907	0.093

α9α10		
Comparison	**seqID**	**1-seqID**
Rat-amniote	0.683	0.317
Chick-amniote	0.821	0.179
Amniote-tetrapod	0.96	0.04
Frog-tetrapod	0.814	0.186

Supplementary Table 7. Estimated distances between extant and inferred ancestral α9α10, α4β2 and α7 nAChRs based on protein sequence identity. Sequence identity (seqID) values between pairs of sequences were calculated using the protein sequence alignments in Supplementary File 3). Distances (1-seqID values) were subsequently used as branch lengths for the receptor trees used for the inference of ancestral character states for each nAChR (Supplementary Figure 6).

Supplementary Files

Supplementary File 1. Multiple alignment of nAChRs subunits. The alignment includes 392 nAChR subunits sequences from 29 different species together with 9 sequences from 5HT3B vertebrate subunits (outgroup).

Supplementary File 2. Sequences used for the reconstruction of ancestral nAChR subunits. DNA sequences from α4, α7, α9, α10 and β2 orthologues used to reconstruct DNA sequences from amniote and tetrapod ancestors. The species trees, in parenthetic format, are shown before the sequence alignment, in fasta format. The branch lengths in the species trees were inferred from each alignment and indicate the amount of accumulated changes.

Supplementary File 3. Extant and inferred ancestral nAChRs protein sequences. Protein sequences from rat, chicken, frog, amniote ancestor and tetrapod ancestor, from α7, $(\alpha4)_2(\beta2)_3$ and $(\alpha9)_2(\alpha10)_3$ nAChRs were aligned and the sequence identity between pairs of receptors was used to calculate the branch lengths assigned to the receptor trees (Supplementary Figure 6) used to infer ancestral character states of biophysical properties (Supplementary Figure 7).